*Mineralogical Magazine, August 2015, Vol. 79(4), pp. 909–939*

# Petrological and geochemical characteristics of Mesoproterozoic dyke swarms in the Gardar Province, South Greenland: Evidence for a major sub-continental lithospheric mantle component in the generation of the magmas

ALEXANDER BARTELS[1,*], TROELS F. D. NIELSEN[1], SEUNG RYEOL LEE[2] AND BRIAN G. J. UPTON[3]

[1] Department of Petrology and Economic Geology, Geological Survey of Denmark and Greenland (GEUS), Øster Voldgade 10, DK-1350 Copenhagen, Denmark
[2] Department of Earth and Planetary Sciences, Geological Research Division, Korea Institute of Geoscience and Mineral Resources, Daejeon 305-350, Korea
[3] University of Edinburgh, School of GeoSciences, West Mains Road, Edinburgh EH9 3JW, UK

[*Received 30 October 2014; Accepted 2 March 2015; Associate Editor: R. Mitchell*]

## ABSTRACT

The Mesoproterozoic Gardar Province in South Greenland developed in a continental rift-related environment. Several alkaline intrusions and associated dyke swarms were emplaced in Archaean and Ketilidian basement rocks during two main magmatic periods at 1300–1250 Ma and 1180–1140 Ma. The present investigation focuses on mafic dykes from the early magmatic period ('Older Gardar') and the identification of their possible mantle sources.

The rocks are typically fine- to coarse-grained dolerites, transitional between tholeiitic and alkaline compositions with a general predominance of Na over K. They crystallized from relatively evolved, mantle-derived melts and commonly show minor degrees of crustal contamination. Selective enrichment of the large ion lithophile elements Cs, Ba and K and the light rare-earth elements when compared to high field-strength elements indicate significant involvement of a sub-continental lithospheric mantle (SCLM) component in the generation of the magmas. This component was affected by fluid-dominated supra-subduction zone metasomatism, possibly related to the Ketilidian orogeny ~500 Ma years prior to the onset of Gardar magmatism. Melt generation in the SCLM is further documented by the inferential presence of amphibole in the source region, negative calculated $\varepsilon_{Nd(i)}$ values (−0.47 to −4.40) and slightly elevated $^{87}Sr/^{86}Sr_{(i)}$ (0.702987 to 0.706472) ratios when compared to bulk silicate earth as well as relatively flat heavy rare-earth element (*HREE*) patterns ($(Gd/Yb)_N$ = 1.4–1.9) indicating melt generation above the garnet stability field.

The dyke rocks investigated show strong geochemical and geochronological similarities to pene-contemporaneous mafic dyke swarms in North America and Central Scandinavia and a petrogenetic link is hypothesized. Considering recent plate reconstructions, it is further suggested that magmatism was formed behind a long-lived orogenic belt in response to back-arc basin formation in the time interval between 1290–1235 Ma.

**KEYWORDS:** dyke petrogeny, Mesoproterozoic, North Atlantic craton, Gardar Province, South Greenland.

* E-mail: a.bartels82@gmail.com
DOI: 10.1180/minmag.2015.079.4.04

This paper is published as part of a special set in *Mineralogical Magazine*, Volume **79(4)**, 2015, arising out of the March 2014 NAC Conference on the North Atlantic Craton.

## Introduction

THE identification of mantle sources of mafic and ultramafic magmatism is essential for the understanding of mantle dynamics and crustal evolution. In continental settings, the fundamental question is whether melts were derived from the sub-continental lithospheric mantle (SCLM), the sub-lithospheric upper mantle, upwelling plume material, or represent mixtures of these individual mantle components. Some workers argue that the lithospheric mantle is too refractory to produce large volumes of basaltic melts and favour a predominantly asthenospheric origin for continental mafic magmatism (White and McKenzie, 1989; Arndt and Christensen, 1992). Others suggest that metasomatically enriched SCLM is sufficiently fertile to facilitate basaltic magma generation (Jordan, 1988; Gallagher and Hawkesworth, 1992; Turner *et al.*, 1996).

A second major debate focuses on whether mantle melting in continental settings is predominantly triggered by 'active' (plume-related) or 'passive' (plate-driven) rifting. In the light of these contrasting views it is important to consider carefully plate reconstruction models in the discussion of intracontinental magmatism.

The Mesoproterozoic Gardar Province of South Greenland formed in a rift-related intra-continental environment between 1300 and 1140 Ma (Upton *et al.*, 2003) along the southern part of the Greenlandic North Atlantic craton (NAC). A more recent geochronological compilation (Upton, 2013) restricts the magmatism to two separated episodes around ~1280 Ma and ~1160 Ma. In terms of the debate of lithospheric *vs.* sub-lithospheric mantle sources described above, it is important to note that the Gardar underlying mantle was influenced by supra-subduction zone metasomatism during the Palaeoproterozoic Ketilidian orogeny (Garde *et al.*, 2002) and several authors have proposed that the magma generation came about through partial melting of the SCLM (Upton and Emeleus, 1987; Upton *et al.*, 2003; Köhler *et al.*, 2009; Upton, 2013). A contrasting interpretation is given by Halama *et al.* (2002, 2004 and 2007) who suggested an increasing dominance of an enriched plume component during the younger Gardar magmatic period with trace-element characteristics similar to common ocean-island basalts (OIB).

This is in agreement with findings from Coulson *et al.* (2003) on minor occurrences of lamprophyric and carbonatitic rocks, emplaced during the younger as well as the older Gardar magmatism. These rocks show significant geochemical and isotopic similarities to typical OIB and a two-step model is suggested by Coulson *et al.* (2003) where small-degree volatile-rich partial melts from the asthenosphere were frozen in as metasomatites in the SCLM, but rapidly remobilized during the magmatism of the Gardar rift.

These studies give evidence that different mantle sources might have been involved in the magmatism. Thus, it is crucial that mafic and ultramafic rocks of the two magmatic periods will be investigated separately to provide as detailed information as possible on the potential mantle reservoirs involved in the Gardar magmatism.

In the present study, mafic dyke swarms of the Older Gardar magmatic activity are investigated geochemically. Isotopic and trace-element data are used to identify possible mantle sources and, together with previously published data, new constraints on the time-dependent evolution of the Gardar magmatic period are made. In addition, possible implications for the early Gardar rift dynamics are discussed in the light of recent plate reconstruction models (Evans and Mitchell, 2011; Johansson, 2013).

## Geological setting

### *The Gardar Province*

The geology of southern Greenland can be subdivided into three major units, the Archaean North Atlantic craton (NAC) in the north, the Palaeo-Proterozoic Ketilidian in the south and the geographically and volumetrically much more restricted intrusions and contemporaneous lavas and sediments of the Mesoproterozoic Gardar Province. Gardar magmas formed in an extensional environment around 500 Ma after the Ketilidian orogeny. Their intrusion was concentrated along the boundary between the NAC and the Ketilidian mobile belt into Archaean as well as the Ketilidian basement rocks during two main magmatic events around ~1280 Ma and ~1160 Ma. Considering their age, the Gardar rocks are remarkably well preserved. They comprise un-metamorphosed and un-deformed intrusive rocks as well as a succession of sediments with interbedded lavas, belonging to the Eriksfjord Formation. The intrusions are principally dykes as well as 14 plutons or plutonic complexes ranging from ~300 m up to 50 km in diameter (Upton *et al.*, 2003). The plutons are



https://doi.org/10.1180/minmag.2015.079.4.04 Published online by Cambridge University Press

dominated by alkaline and peralkaline rocks, with syenites and nepheline syenites as the most abundant rock types.

The associated dyke swarms show a significant petrographic range from olivine gabbros and dolerites to quartz syenites and alkali granites (Upton *et al.* 2003; Köhler *et al.*, 2009). Lamprophyric and carbonatitic dykes are less common but occur in several areas of the province (Coulson *et al.*, 2003; Upton *et al.*, 2006).

### *Brown Dykes ($BD_0$, $BD_1$ and $BD_2$)*

During the early period of magmatism (~1280 Ma) the largest group of dykes in number, volume and extent are the 'Brown Dykes' (BD) which are the subject of this study. Wegmann (1938) referred to them by this name on account of their typical brown weathering colour. They can be observed throughout the province, intruding both the Archaean and the Ketilidian basement rocks. Based on a large number of cross-cutting relationships, three suites have been distinguished. In the literature they are identified by suffixes indicative of their relative ages ($BD_0$, $BD_1$ and $BD_2$ (Berthelsen and Henriksen, 1975)). The abundance of BD is greatest in the area around and north of Ivittuut within the Archaean basement rocks (Fig. 1). A general change of strike from SW–NE strike in the north, to E–W and WNW–ESE strike towards the south can be observed for all three dyke generations throughout the whole rift. Other dykes commonly related to the $BD_0$ generation include WNW–ESE trending olivine dolerites in Johan Dahl Land north of Narsarsuaq and in the area south of Igaliku town (Fig. 1; Allaart, 1969). Within the Isortoq and Julianehåb regions, only the $BD_0$ dyke generation is described and represented by three major and several smaller dykes with a general coast-parallel NW–SE trend. From north to south they can be traced for more than 200 km and curve into an E–W direction before they die out in the area southeast of Qaqortoq (Fig. 1). The U-Pb baddeleyite ages of $BD_0$ dykes range from 1279±1.3 to 1284±3.0 Ma (Upton, 2013).

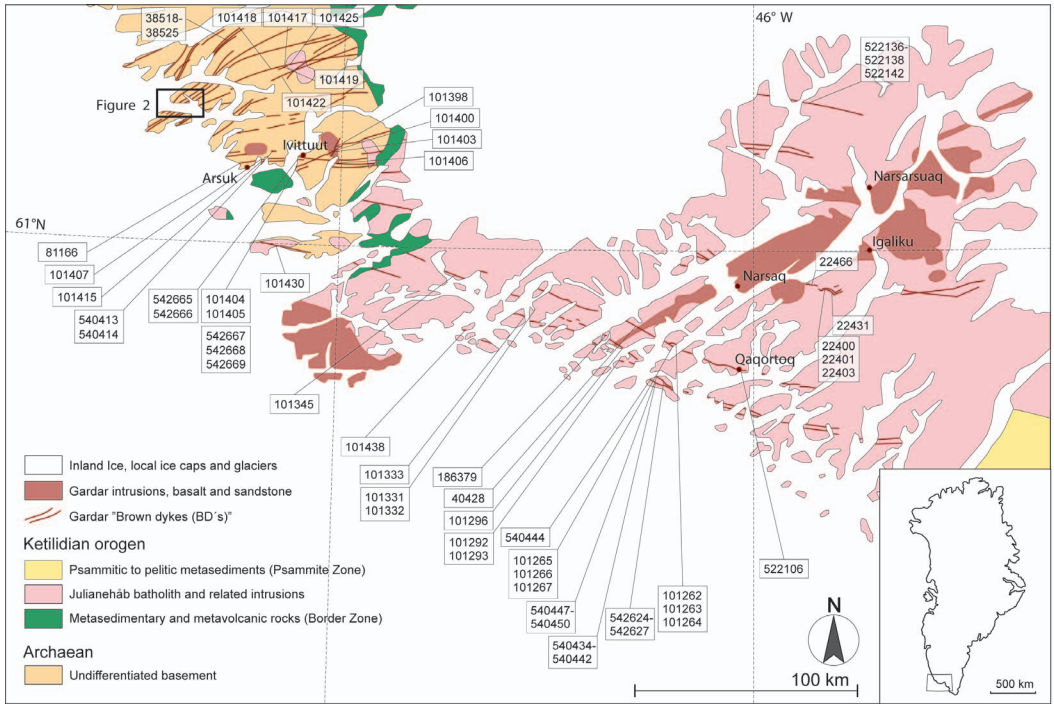


FIG. 1. Simplified geological map showing sample localities and the distribution of 'brown dykes' (BD) in the Gardar Igneous Province, South Greenland based on the work of Berthelsen and Henriksen (1975). Indicated dykes are not to scale. The area marked with a square is enlarged in Fig. 2.



https://doi.org/10.1180/minmag.2015.079.4.04 Published online by Cambridge University Press

## Methods

### *Sampling*

In this study, sample localities were identified based on maps of Berthelsen and Henriksen (1975) and various field maps (Berthelsen, 1958; Bondesen, 1957, 1958; Walton, 1963) from the initial mapping period of the area.

Ninety dyke samples and three samples of basement rocks are included in the present study. Forty-nine of the samples were collected by J. H. Allaart, S. N. Ayrton, C. J. Emeleus and B. G. J. Upton during earlier field investigations between 1958 and 1969 and made available for this study by Asger Ken Pedersen (Natural History Museum of Denmark). In addition, 44 samples from a broad area of the Gardar Province were collected by the first author during two field investigations in 2013. At most localities, samples were collected from both the margin and the centre of the dykes. The complete sample set includes representative samples of all three dyke generations ($BD_0$, $BD_1$ and $BD_2$) which intruded the Archaean basement in the northwest of the Province as well as the described $BD_0$ dykes in the area from Ivittuut to Qaqortoq, south of Igaliku town and from Johan Dahl Land (Figs 1 and 2). Sample numbers, classification and coordinates for samples collected during field investigations in 2013 are given in Table 1.

### *Analytical methods*

Prior to the analyses the samples were cut and weathered surfaces were removed. Thin-sections (~30–100 μm thick) were prepared by the Vancouver GeoTech Labs in British Columbia, Canada. Samples were analysed for major and trace elements at ACTLabs in Ontario, Canada (whole-rock geochemistry, analytical packages *4Lithoresearch* and *4B2 research*). Prior to analysis the samples were crushed using the mild-steel method. The analytical procedure includes dilution of lithium metaborate/tetraborate fused samples followed by analysis on a Perkin Elmer SCIEX ELAN 6000, 6100 or 9000 inductively coupled plasma mass spectrometer. The major oxide components and trace elements of 32 samples were previously determined at the University of Edinburgh using X-ray fluorescence (XRF) analysis (samples are marked with a star on electronic Table 2, which has been deposited

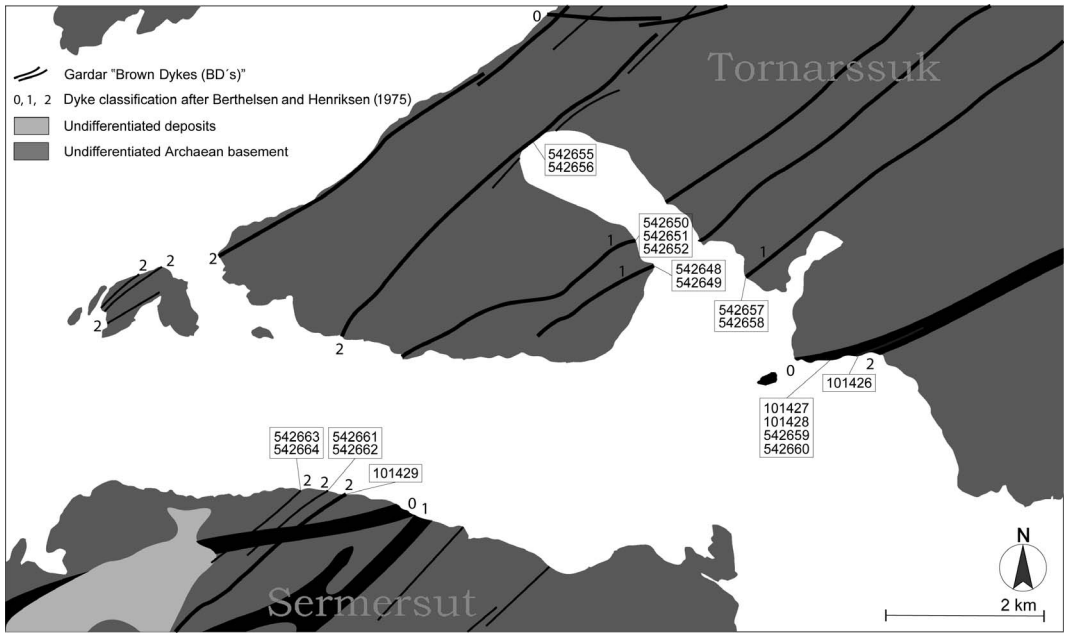


FIG. 2. Sketch map showing sample localities at the SW coast of Tornarssuk and N coast of Sermersut. Brown dykes of the different generations identified by Berthelsen and Henriksen (1975) are indicated by given numbering (0, 1 and 2).



https://doi.org/10.1180/minmag.2015.079.4.04 Published online by Cambridge University Press

TABLE 1. Samples collected during field investigations in 2013.

| Sample | Generation | Latitude | Longitude |
|---|---|---|---|
| 540413 | $BD_{0Arch}$ | 61.217717º | –48.375167º |
| 542659 | $BD_{0Arch}$ | 61.315067º | –48.703333º |
| 542660 | $BD_{0Arch}$ | 61.315067º | –48.703333º |
| 542665 | $BD_{0Arch}$ | 61.200183º | –48.201817º |
| 542666 | $BD_{0Arch}$ | 61.200183º | –48.201817º |
| 542648 | $BD_1$ | 61.325217º | –48.737033º |
| 542649 | $BD_1$ | 61.325217º | –48.737033º |
| 542650 | $BD_1$ | 61.328867º | –48.742533º |
| 542651 | $BD_1$ | 61.328867º | –48.742533º |
| 542652 | $BD_1$ | 61.328867º | –48.742533º |
| 542657 | $BD_1$ | 61.324733º | –48.714850º |
| 542658 | $BD_1$ | 61.324733º | –48.714850º |
| 542667 | $BD_1$ | 61.188983º | –48.212150º |
| 542668 | $BD_1$ | 61.188983º | –48.212150º |
| 542669 | $BD_1$ | 61.188983º | –48.212150º |
| 542655 | $BD_2$ | 61.339000º | –48.762383º |
| 542656 | $BD_2$ | 61.339000º | –48.762383º |
| 542661 | $BD_2$ | 61.299083º | –48.816117º |
| 542662 | $BD_2$ | 61.299083º | –48.816117º |
| 542663 | $BD_2$ | 61.298433º | –48.808483º |
| 542664 | $BD_2$ | 61.298433º | –48.808483º |
| 522106 | BD | 60.718983º | –46.036217º |
| 522136 | BD | 61.349667º | –45.730183º |
| 522137 | BD | 61.349667º | –45.730183º |
| 522138 | BD | 61.349667º | –45.730183º |
| 540434 | $BD_{0Ket}$ | 60.702133º | –46.462467º |
| 540437 | $BD_{0Ket}$ | 60.702367º | –46.463833º |
| 540438 | $BD_{0Ket}$ | 60.702367º | –46.463833º |
| 540439 | $BD_{0Ket}$ | 60.702367º | –46.463833º |
| 540440 | $BD_{0Ket}$ | 60.702367º | –46.463833º |
| 540441 | $BD_{0Ket}$ | 60.702367º | –46.463833º |
| 540442 | $BD_{0Ket}$ | 60.702367º | –46.463833º |
| 540444 | $BD_{0Ket}$ | 60.703917º | –46.468033º |
| 540447 | $BD_{0Ket}$ | 60.705567º | –46.441117º |
| 540448 | $BD_{0Ket}$ | 60.706133º | –46.442617º |
| 540449 | $BD_{0Ket}$ | 60.706000º | –46.441167º |
| 540450 | $BD_{0Ket}$ | 60.705250º | –46.439550º |
| 542624 | $BD_{0Ket}$ | 60.696833º | –46.408933º |
| 542625 | $BD_{0Ket}$ | 60.696833º | –46.408933º |
| 542626 | $BD_{0Ket}$ | 60.696833º | –46.408933º |
| 542627 | $BD_{0Ket}$ | 60.696833º | –46.408933º |

with the Principal Editor of *Mineralogical Magazine* and is available from www.minersoc.org/pages/e_journals/dep_mat_mm.html). For 20 of these samples, the major-element compositions are reported here together with new trace-element determinations using the above mentioned method (*4B2-research*). Scandium (Sc) and lead (Pb) are not included in the commercial package offered by ACTLabs and the concentrations of these two elements are taken from the XRF analyses.

For Rb-Sr and Sm-Nd isotope analyses, sample powders of ~100 mg were spiked with mixed $^{87}Rb$-$^{84}Sr$ and $^{149}Sm$-$^{150}Nd$ tracers and dissolved



https://doi.org/10.1180/minmag.2015.079.4.04 Published online by Cambridge University Press

in PFA Teflon vessels at a sub-boiling temperature for two or three days with HF + $HClO_4$ acid. After complete dissolution, the solution was dried, dissolved in 0.5 ml of 2.5 M HCl and then centrifuged before loading into the column. The Rb, Sr and the *REE* were separated by conventional cation-exchange techniques (DOWEX 50WX8 resin) with 2.5 M and 6 M HCl as eluant. The separation of Nd and Sm from the bulk *REE* was performed on quartz-glass columns using EICHROM LN resin with 0.25 M and 0.5 M HCl as eluant. Rubidium, Sr, Sm and Nd isotopic compositions were measured using a TRITON-plus thermal ionization mass spectrometer at the Korea Institute of Geoscience and Mineral Resources. For Sr and Nd isotopic ratios, the mass fractionation corrections were based on $^{86}Sr/^{88}Sr = 0.1194$ and $^{146}Nd/^{144}Nd = 0.7219$, respectively. Replicate analyses of NBS-987 Sr and JNdi-1 Nd standards gave $^{87}Sr/^{86}Sr = 0.710242 \pm 0.000004$ ($2\sigma$, $n = 5$) and $^{143}Nd/^{144}Nd = 0.512102 \pm 0.000002$ ($2\sigma$, $n = 5$), respectively, during this analytical session. Total procedural blanks were <200 pg for Rb, Sm and Nd, and 4.5 ng for Sr. Analytical uncertainties (two standard errors measured or calculated) are estimated approximately to be 0.002% or better for $^{143}Nd/^{144}Nd$, 0.3% or better for $^{87}Rb/^{86}Sr$, except for samples 542625 (<0.8%), 101331 (<0.6%) and 101429 (<0.5%), and 0.2% or better for $^{147}Sm/^{144}Nd$, except for samples 542625 (<1%) and 542648 (<0.5%). Because of the relatively high blank level for Sr, approximately half of the analytical uncertainties on $^{87}Sr/^{86}Sr$ ratios reported here are contributed from the blank correction (Table 3).

## Results

In the presentation of the analytical results, the classic subdivision of the dykes in generations $BD_0$, $BD_1$ and $BD_2$ (Berthelsen and Henriksen, 1975) has been maintained. Based on their strike direction and host rocks, the $BD_0$ generation was grouped further into dykes intruding the Archaean basement in the northern parts of the Province ($BD_{0Arch}$) and dykes intruding the Proterozoic Ketilidian basement in the south of the Province ($BD_{0Ket}$).

### *Field observations and petrography*

All the dykes investigated are sub-vertical and their widths vary from a few cm up to hundreds of metres but are commonly between 5 and 20 m. Within all three generations, small sub-swarms and apophyses can be observed, which are, on close inspection, commonly related to the terminations of dykes. The crustal dilation in the Ivittuut region is, on the basis of the accumulated widths of the dykes, estimated to have been ~3% (Berthelsen and Henriksen (1975).

The dykes typically have very fine-grained chilled margins and a symmetrical increase in grain-size towards the dyke centre can be observed. Within some of the bigger dykes (>20 m wide), there are pegmatitic pockets and veins. In some of the marginal facies, granitic veins indicate melting and back-veining of basement rocks during dyke-emplacement. A more detailed description of emplacement and field characteristics of the BD is given by Ayrton (1963) and Berthelsen and Henriksen (1975).

All the samples investigated are holocrystalline and textures typically range from aphyric to porphyritic. Porphyritic samples are characterized by poikilitic to sub-poikilitic clinopyroxene enclosing plagioclase with or without olivine and Fe-Ti-oxides (Fig. 3*a*). Flow lamination of the major mineral assemblage as well as accumulation of olivine and plagioclase within dyke margins can be observed in some samples (Fig. 3*b*,*d*). Large (up to 1.5 cm) plagioclase pheno- or xenocrysts occur occasionally (Fig. 3*c*). Samples from chilled margins indicate additionally the occurrence of two generations of plagioclase pheno- and/or xenocrysts (Fig. 3*d*).

In order of abundance, the major magmatic phases are idiomorphic plagioclase (40–60 vol.%), interstitial clinopyroxene (15–35 vol.%), subhedral olivine (15–25 vol.%) and Fe-Ti oxides (5–15 vol.%). Biotite and euhedral apatite are minor components and most likely crystallized at a late stage. Small (typically ~10–200 μm) crystallized sulfide globules can be found in most of the samples. Additional accessory phases are identified as titanite, zircon, baddeleyite and monazite. Secondary alteration results in sericitization of plagioclase and chlorite replacing pyroxenes and/or interstitial glass. Mineral abbreviations used in the following are based on the classification of Kretz (1983).

### *Whole-rock geochemistry*

Despite the occurrence of phenocrysts or xenocrysts in some of the samples, whole-rock data listed in electronic Table 2 (deposited with the



https://doi.org/10.1180/minmag.2015.079.4.04 Published online by Cambridge University Press

TABLE 3. Sr and Nd isotopic composition of dyke rocks and adjacent Archaean and Ketilidian basement rocks.

| Sample | Rb (ppm) | Sr (ppm) | $^{87}Rb/^{86}Sr$ | $^{87}Sr/^{86}Sr$ | 2σ | Sm (ppm) | Nd (ppm) | $^{147}Sm/^{144}Nd$ | $^{143}Nd/^{144}Nd$ | 2σ | $\varepsilon_{Nd}$ (i) | $^{87}Sr/^{86}Sr$ (i) |
|---|---|---|---|---|---|---|---|---|---|---|---|---|
| 542625 | 7.68 | 436.4 | 0.04965 | 0.704651 | 0.000020 | 2.61 | 11.44 | 0.14350 | 0.512040 | 0.000008 | −2.93 | 0.703737 |
| 542626 | 7.46 | 359.5 | 0.05852 | 0.704511 | 0.000027 | 4.12 | 18.01 | 0.14396 | 0.512095 | 0.000008 | −1.91 | 0.703434 |
| 101345 | 6.91 | 367.8 | 0.05303 | 0.704382 | 0.000050 | 3.75 | 16.35 | 0.14433 | 0.512080 | 0.000008 | −2.27 | 0.703406 |
| 101331 | 8.09 | 394.4 | 0.05785 | 0.704410 | 0.000026 | 3.38 | 14.86 | 0.14333 | 0.512118 | 0.000008 | −1.36 | 0.703345 |
| 542648 | 3.36 | 397.6 | 0.02383 | 0.703636 | 0.000027 | 2.25 | 9.32 | 0.15215 | 0.512238 | 0.000007 | −0.47 | 0.703197 |
| 542655 | 7.74 | 343.9 | 0.06351 | 0.704880 | 0.000028 | 3.74 | 15.53 | 0.15170 | 0.512234 | 0.000007 | −0.47 | 0.703712 |
| 101429 | 7.31 | 357.1 | 0.05776 | 0.704707 | 0.000029 | 3.25 | 13.62 | 0.15011 | 0.512184 | 0.000007 | −1.19 | 0.703644 |
| 542667 | 4.72 | 524.0 | 0.02542 | 0.703455 | 0.000021 | 3.47 | 14.43 | 0.15135 | 0.512114 | 0.000010 | −2.76 | 0.702987 |
| 542659 | 17.00 | 334.4 | 0.14345 | 0.707881 | 0.000040 | 5.22 | 24.57 | 0.13375 | 0.511976 | 0.000006 | −2.56 | 0.705242 |
| 542660 | 14.97 | 251.4 | 0.16805 | 0.709564 | 0.000033 | 5.60 | 25.71 | 0.13723 | 0.511991 | 0.000011 | −2.86 | 0.706472 |
| 540437 | 11.51 | 404.0 | 0.08039 | 0.706059 | 0.000027 | 3.78 | 18.46 | 0.12876 | 0.511876 | 0.000008 | −3.70 | 0.704580 |
| 540444 | 16.48 | 384.3 | 0.12097 | 0.706939 | 0.000029 | 5.05 | 24.29 | 0.13090 | 0.511858 | 0.000007 | −4.40 | 0.704713 |
| 540435 | 117.92 | 652.9 | 0.51012 | 0.715996 | 0.000022 | 8.26 | 50.89 | 0.10215 | 0.511627 | 0.000007 | −4.19 | 0.706610 |
| 540414 | 66.82 | 183.7 | 1.03064 | 0.748938 | 0.000070 | 5.38 | 35.70 | 0.09481 | 0.510870 | 0.000008 | −17.78 | 0.729974 |

The $^{87}Sr/^{86}Sr$ and $^{143}Nd/^{144}Nd$ were normalized to 0.1194 and 0.7219, respectively, after spike and blank corrections.
NBS987 Sr STD = 0.710242 +/− 0.000004 (2σ, $n$ = 5), JND−1 ND STD = 0.512102 +/− 0.000002 (2σ, $n$ = 5).
Errors in Rb/Sr <0.3%, 2σ except for samples 542625 (<0.8%, 2σ), 101331 (<0.6%, 2σ) and 101429 (<0.5%, 2σ).
Errors in Sm/Nd <0.1%, 2σ except for samples 542625 (<1%, 2σ), 542648 (<0.5%, 2σ), 101331 and 101429 (<0.2%, 2σ).
Initial Sr and Nd isotopic compositions along with εNd(i) values were calculated for an emplacement age of 1285 Ma.

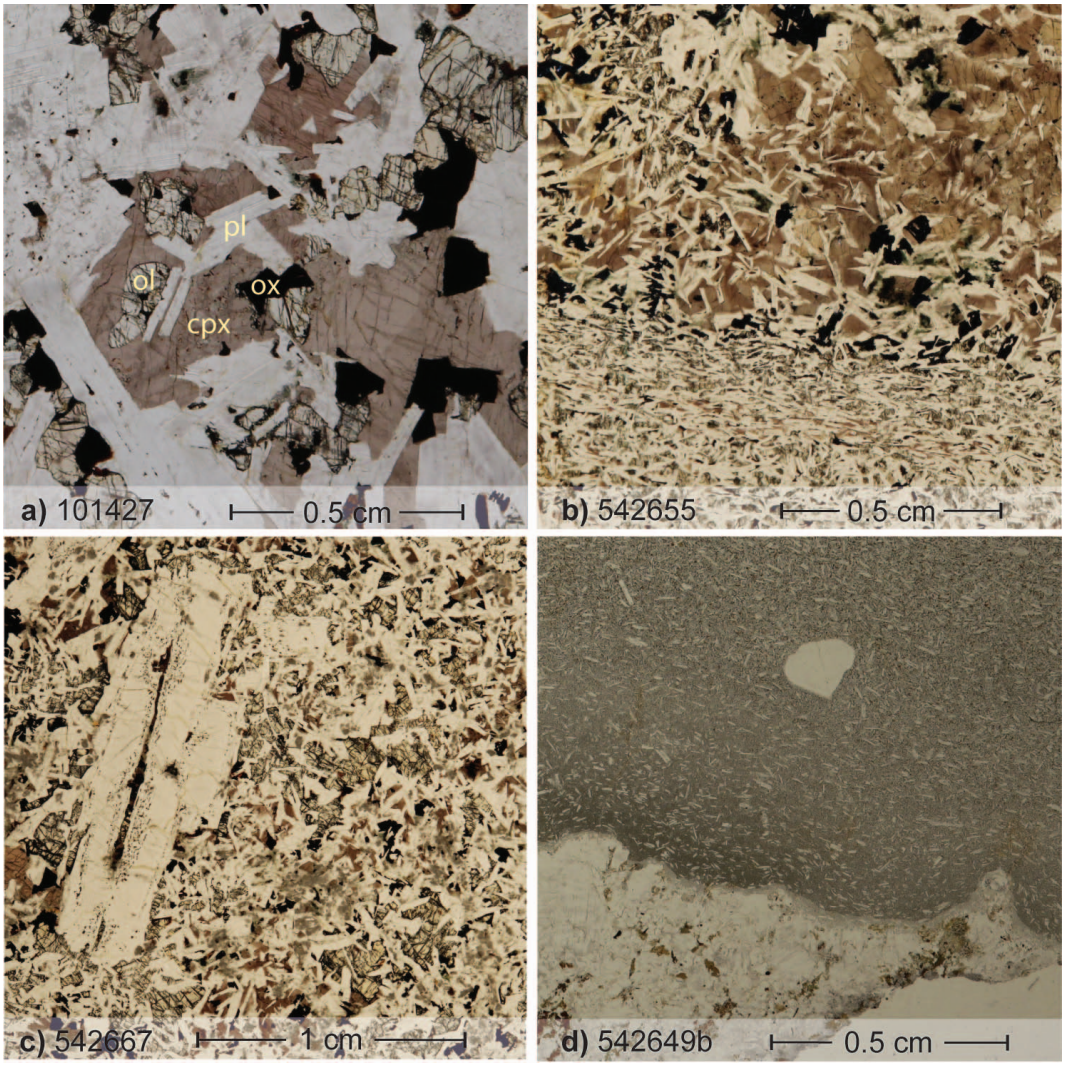


FIG. 3. Photomicrographs showing typical textures observable in the dyke rocks investigated. (*a*) Large poikilitic clinopyroxene hosting plagioclase, olivine and Fe-Ti-oxides (101427). (*b*) Flow lamination in marginal sample (542655). Olivine and plagioclase are accumulated in the lower parts and the latter is clearly flow oriented. (*c*) Typical dolerite texture in a medium grained dyke with a large (~1.5 cm) plagioclase pheno-/xenocryst (542667). (*d*) Chilled margin against Archaean basement (lower part). The rock is very fine grained and hosts abundant plagioclase phenocrysts. Along the margin, the phenocrysts are oriented showing flow lamination. A second generation of phenocrysts is represented by a larger plagioclase (542649b). Key – pl: plagioclase, ol: olivine, cpx: clinopyroxene, ox: oxides. The images are taken from thick sections (~100 μm).

Principal Editor of *Mineralogical Magazine* and available from www.minersoc.org/pages/e_journals/dep_mat_mm.html) may be regarded as close approximations to the parental melt of the dykes investigated. Loss on ignition (LOI) values of the analyses vary between 0 and 3.7 with a median (m) value of 0.2 wt.%. The common major- and trace-element characteristics described in the following are based on the sum of all the analytical data and individual trends for the specific dyke swarms ($BD_{0Arch}$, $BD_1$, $BD_2$ and



https://doi.org/10.1180/minmag.2015.079.4.04 Published online by Cambridge University Press

$BD_{0Ket}$) are mentioned only when they deviate significantly from the observed major trends. An attempt to discriminate between the individual BD swarms based on whole-rock geochemistry is presented below.

The dykes have $SiO_2$ contents between 42 and 52 wt.% and alkali contents ($Na_2O + K_2O$) vary between 2.89 and 6.12 wt.% with a general predominance of Na over K. In the revised (after Pearce, 1996) chemical classification diagram after Winchester and Floyd (1977), the majority of the samples investigated plot in the field of basalts and follow a vertical trend towards the field of andesites and basaltic andestites (Fig. 4) consistent with the fractionation of plagioclase + olivine + augite + magnetite. Five samples which were collected from chilled margins plot in the fields of andesite and basaltic andesite. In the $FeO_{(t)}$–$Na_2O$+$K_2O$–MgO ternary plot after Irvine and Baragar (1971), the majority of the samples follow a trend towards larger iron concentrations similar to that of tholeiites. However, the compositions are close to the boundary lines between calc-alkaline and tholeiitic trends and even some of the samples show affinities towards a calk-alkaline trend with increased alkali concentrations (Fig. 5).

Calculated magnesium numbers (Mg# = 100*Mg/(Mg+$Fe^{2+}$); with total iron expressed as $Fe^{2+}$) vary between 22 and 60. Variation diagrams of major oxides, selected trace elements and element ratios, plotted against Mg#, used as a proxy for melt evolution, are illustrated in Figs 6 and 7 and are used in the discussion to identify possible fractionation trends. Primitive mantle-normalized multi-element diagrams of incompatible elements are shown in Fig. 8*a*–*d* for the individual dyke swarms ($BD_{0Arch}$, $BD_1$, $BD_2$ and $BD_{0Ket}$). For simplicity, some of the data, mainly of marginal samples, are excluded in the multi-element plots and will be discussed separately. Also excluded are two samples that show extremely negative Nb anomalies (522137 and 522138) as well as sample 101398 which is highly enriched in all of the incompatible elements. All of the patterns shown have remarkable negative anomalies of high field-strength elements (HFSE) such as Th, U, Ta, Nb and to a minor extent Hf and Y when compared to some of the large ion lithophile elements (LILE), e.g. Cs, Ba and K which tend to be enriched. Strontium exhibits positive anomalies for the most primitive samples which decrease with increasing fractionation and turn into negative anomalies for the middle to

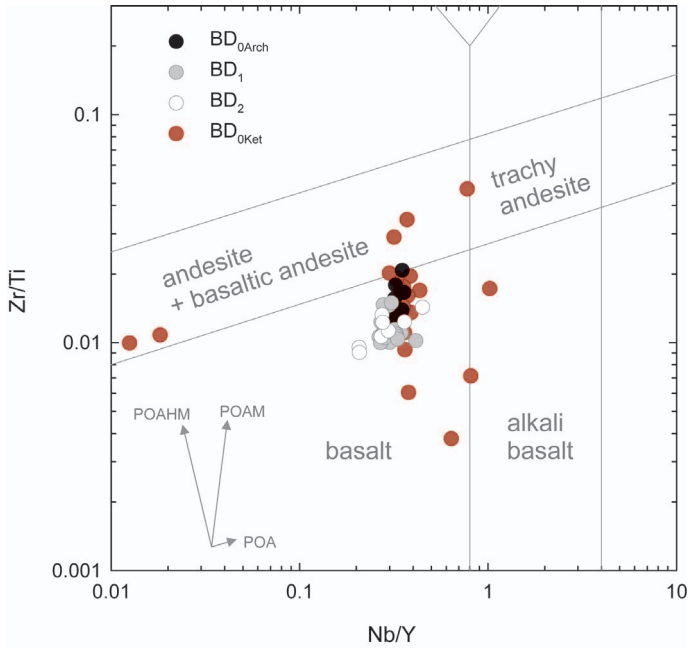


FIG. 4. Zr/Ti *vs.* Nb/Y discrimination diagram of Winchester and Floyd (1977) with revised fields after Pearce (1996). Fractionation vectors: POA = plagioclase + olivine + augite, POAM = plagioclase + olivine + augite + magnetite, POAHM = plagioclase + olivine + augite + hornblende + magnetite.



https://doi.org/10.1180/minmag.2015.079.4.04 Published online by Cambridge University Press

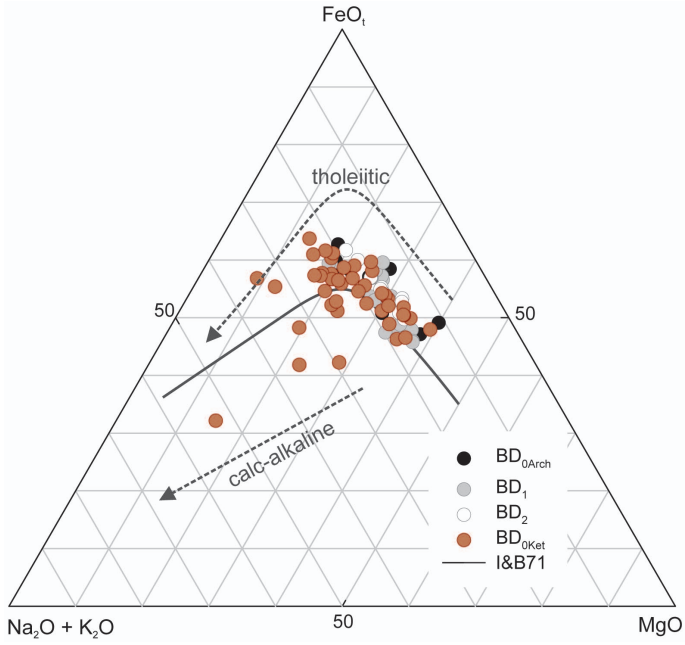


FIG. 5. An AFM discrimination diagram for whole-rock data of the dyke rocks investigated. The solid line after Irvine and Baragar (1971) (I&B71) discriminates between the tholeiitic and calc-alkaline trends (dashed lines). A: ($Na_2O + K_2O$); F: $FeO_t$ ($FeO_t = FeO + 0.8998 * Fe_2O_3$); M: MgO.

highly fractionated samples. Commonly, the $BD_0$ dykes exhibit a higher enrichment in incompatible elements and their negative Sr anomalies are more pronounced than in all other BD compositions (Fig. 8*a*,*d*). Sample 540448 from a chilled margin of a $BD_{0Ket}$ displays an extreme depleted character compared to the other samples (Fig. 8*d*), but with selective enrichment of the LILE and Ti.

Chondrite-normalized *REE* plots display a significant enrichment of *REE* which is more pronounced for the light rare-earth elements (*LREE*) with La abundances between 11–167 times chondritic values (Fig. 9*a*–*d*). From La to Ho a constantly decreasing trend for the normalized values is observed. The *HREE* show a comparable flat pattern with similar enrichment factors for Ho to Lu between 4 and 31 times chondritic values. All samples show a small decrease in normalized Sm values. The most primitive samples always display a positive Eu-anomaly, which decreases with increasing abundance of *REE*. Negative Eu anomalies occur only in some of the most fractionated samples of the $BD_0$ generation (Fig. 9*a*,*d*). Sample 540448 shows constant *LREE* enrichment with ~11 times chondritic values for La to Sm, a positive Eu anomaly and a decreasing trend of normalized *REE* values from Gd to Lu (Fig. 9*d*).

### *Radiogenic Isotopes*

Based on whole-rock geochemistry, a sub-set of 14 samples was selected for isotopic determinations. The sub-set includes the most primitive samples (with Mg# > 52) of the three main dyke generations described by Ayrton (1963). In addition, and for evaluation of the extent of crustal contamination, four mafic dyke samples with elevated $(Th/Nb)_N$ (used as an indicator for crustal contamination) and one representative sample from the Archaean and one from the Ketilidian basement have been selected.

Strontium and Nd isotopic compositions and related parent-daughter element concentrations of the samples investigated are given in Table 3. Initial Sr and Nd isotopic compositions along with $\varepsilon_{Nd(i)}$ values were calculated for an emplacement age of 1285 Ma (Upton *et al.*, 2003). $\varepsilon_{Nd(i)}$ values for chondritic uniform reservoir (CHUR) and the initial $^{87}Sr/^{86}Sr$ ratio for bulk silicate Earth (BSE) were calculated using present day ratios of $^{143}Nd/^{144}Nd = 0.512638$ (Goldstein *et al.*, 1984)



https://doi.org/10.1180/minmag.2015.079.4.04 Published online by Cambridge University Press

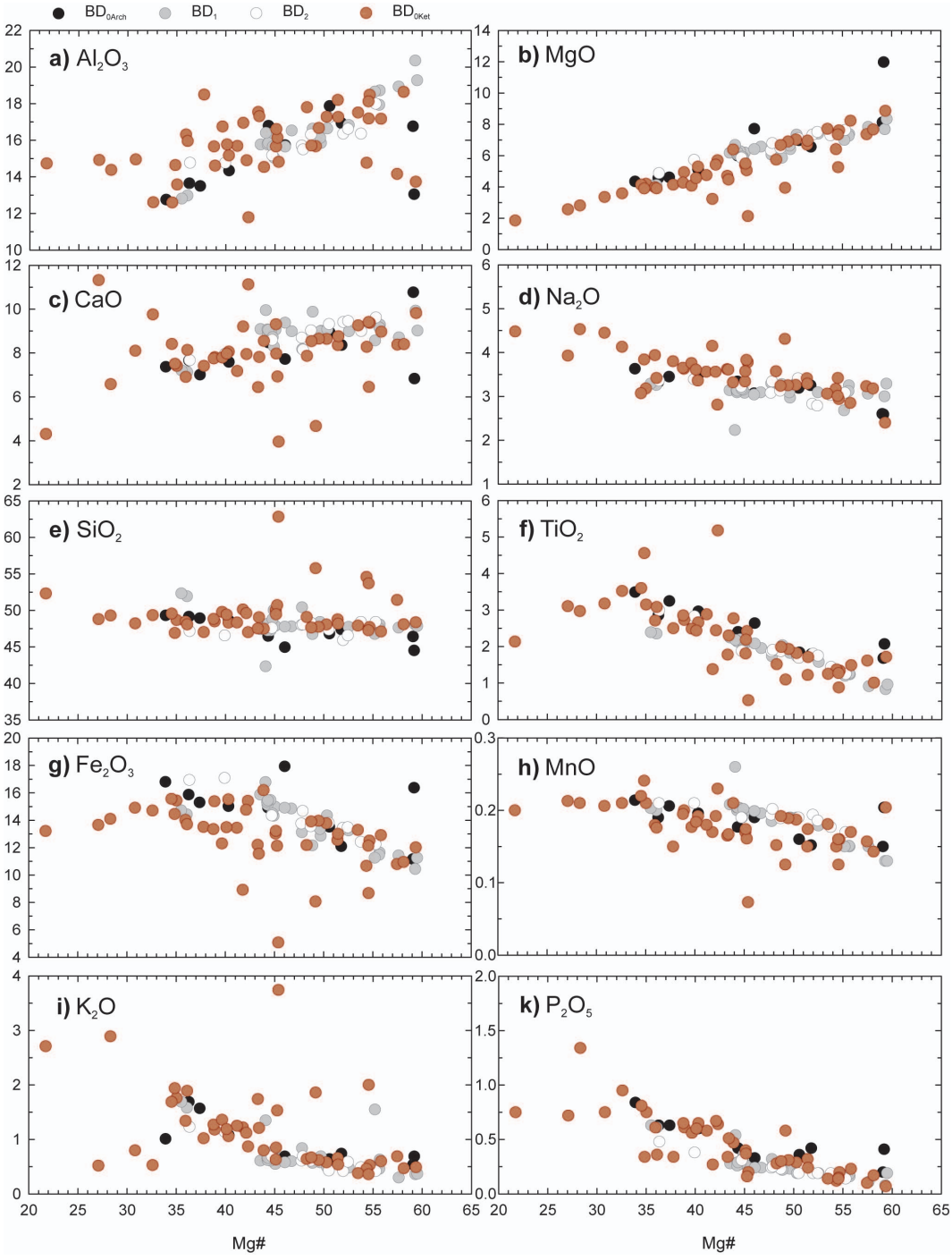


FIG. 6. Major-element variation diagrams for whole-rock data of the dyke rocks investigated with Mg# = 100*Mg/(Mg+$Fe^{2+}$) (with total iron expressed as $Fe^{2+}$) used as fractionation index.



https://doi.org/10.1180/minmag.2015.079.4.04 Published online by Cambridge University Press

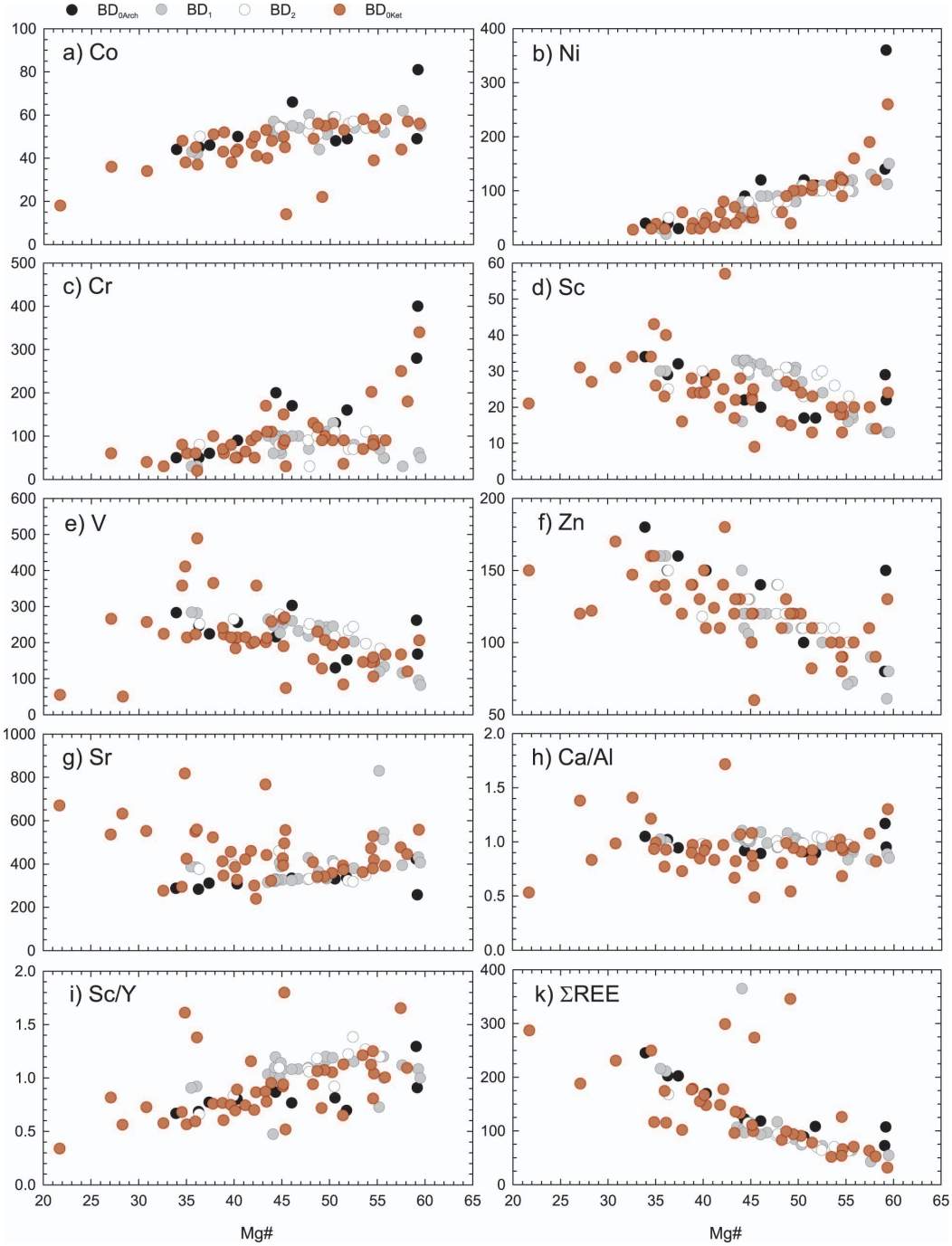


FIG. 7. Trace element (*a*–*g*) and element ratio (*h* and *i*) variation diagrams for whole rock data of the investigated dyke rocks with Mg# = 100*Mg/(Mg+$Fe^{2+}$) (with total iron expressed as $Fe^{2+}$) used as fractionation index. (*k*) Sum of *REE* against Mg#. Most of the samples which are deviating significantly from the trends described in the text can be attributed to marginal samples and contamination with basement material (e.g. the four negative outliers in Fig. 7*a* as well as the three positive outliers in Fig. 7*k* of the $BD_{0Ket}$ generation).



https://doi.org/10.1180/minmag.2015.079.4.04 Published online by Cambridge University Press

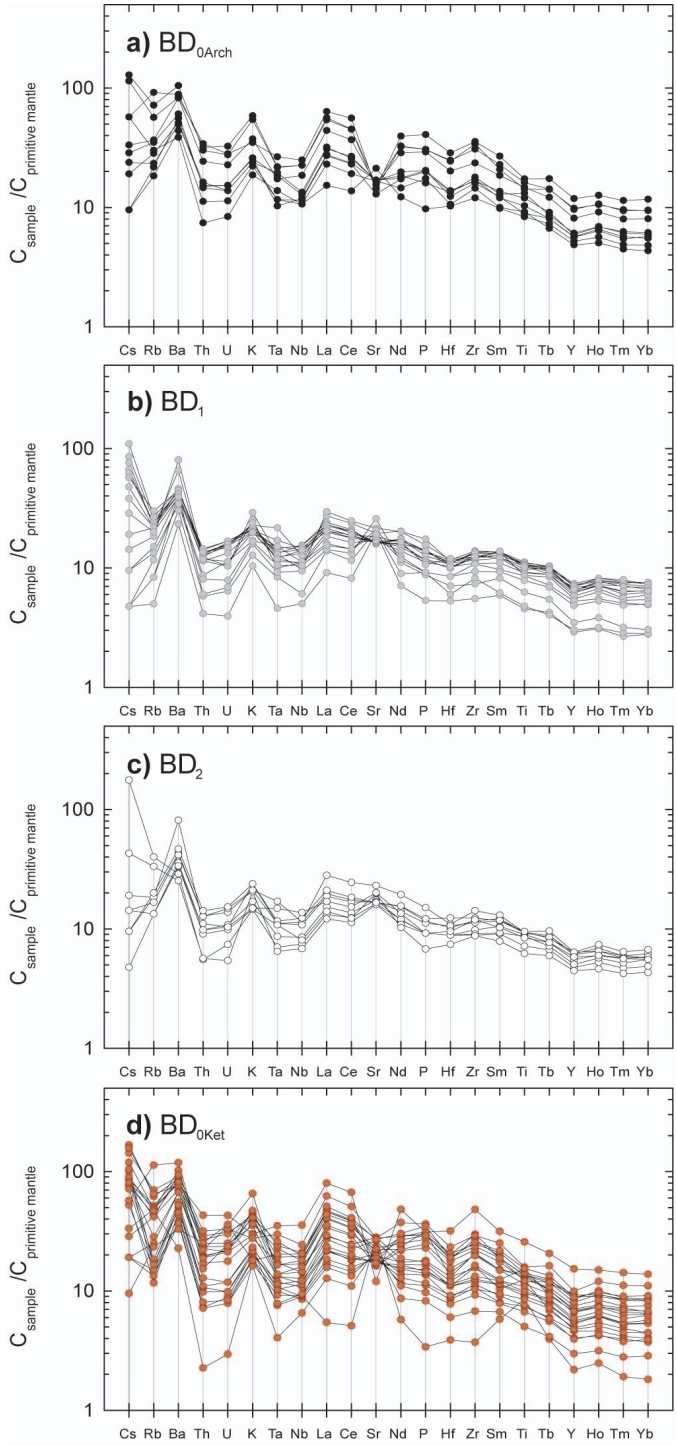


FIG. 8. Multi-element plot of incompatible trace elements for whole-rock samples of the dykes investigated, normalized to primitive mantle values from McDonough and Sun (1995).



https://doi.org/10.1180/minmag.2015.079.4.04 Published online by Cambridge University Press

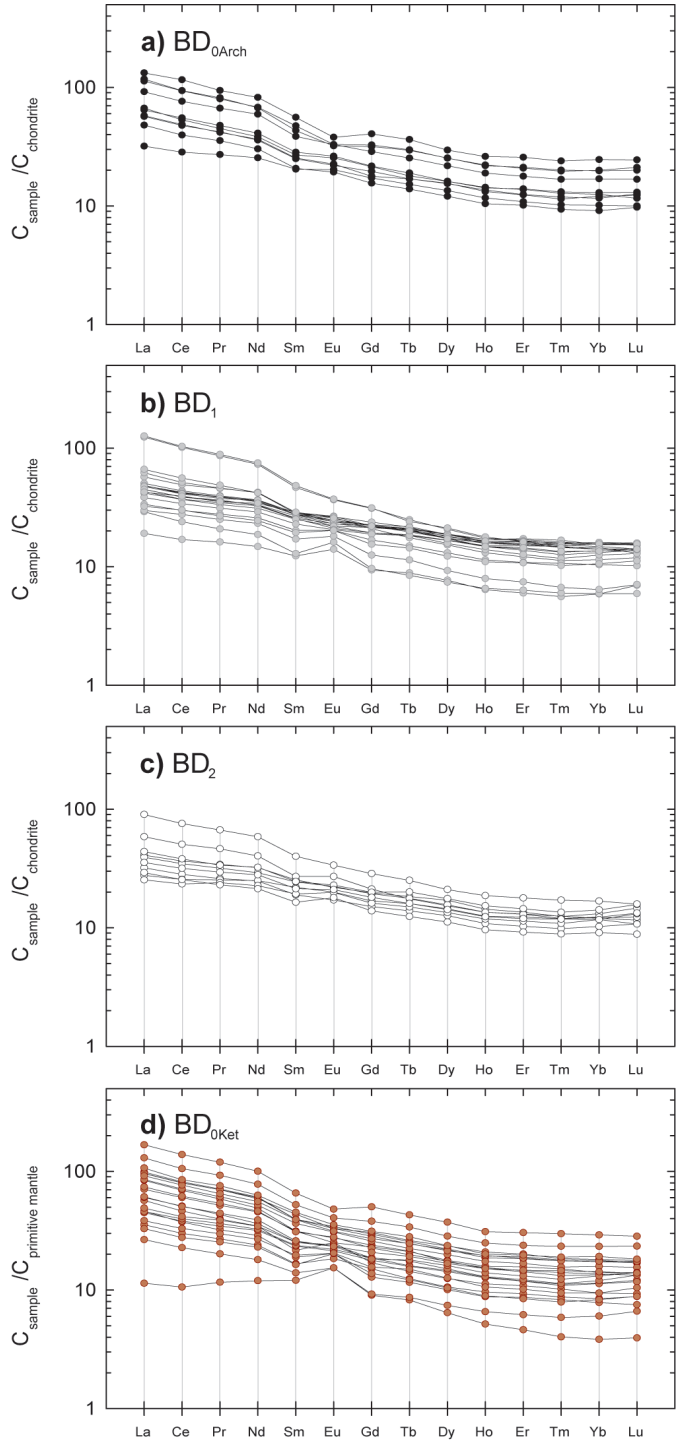


FIG. 9. Rare-earth element plot for whole-rock samples of the dykes investigated, normalized to chondrite values from Boynton (1984).



https://doi.org/10.1180/minmag.2015.079.4.04 Published online by Cambridge University Press

and $^{147}Sm/^{144}Nd$ = 0.1967 (Jacobsen and Wasserburg, 1980) and $^{87}Sr/^{86}Sr$ = 0.745 and $^{87}Rb/^{86}Sr$ = 0.0827 (DePaolo, 1988), respectively.

All the dyke samples have negative $\varepsilon_{Nd(i)}$ values (−0.47 to −4.40) and $^{87}Sr/^{86}Sr_{(i)}$ ratios between 0.702987 and 0.706472 (Fig. 10). In the $\varepsilon_{Nd(i)}$ *vs.* $^{87}Sr/^{86}Sr_{(i)}$ diagram, the majority of the samples describe a narrow isotopic range with slightly larger $^{87}Sr/^{86}Sr_{(i)}$ values (0.702987 to 0.703737) when compared to the calculated BSE value of 0.702978. However, samples with higher $(Th/Nb)_N$ ratios show a clear tendency towards a larger $^{87}Sr/^{86}Sr_{(i)}$ value and describe a trend towards measured values for the respective basement rocks (Fig. 10). Thus the $(Th/Nb)_N$ ratio can, as assumed, be used as a measure for crustal contamination of samples, where isotope data is lacking.

Initial Nd and Sr isotopic compositions from various rock types of the older Gardar magmatic period, taken from previous studies, were calculated for an emplacement age of 1285 Ma and are shown for comparison. These include lower basaltic lavas of the Eriksfjord Formation (Halama *et al.*, 2003), lamprophyres and basalts from the Ivittuut region (Goodenough *et al.*,

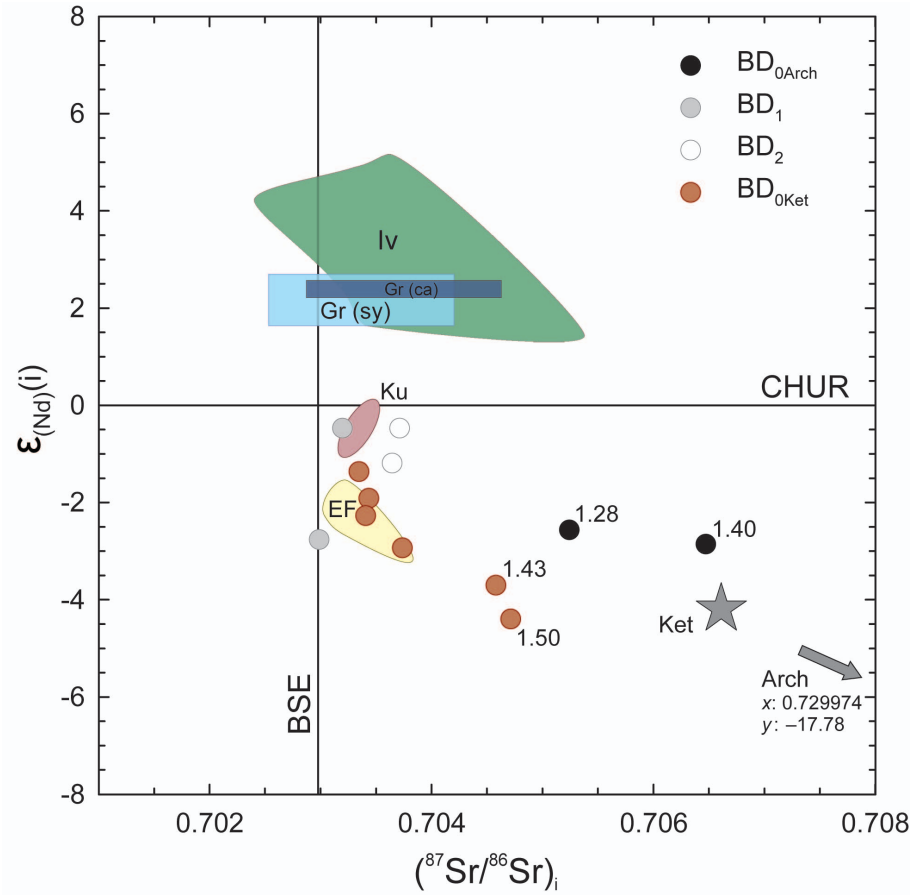


FIG. 10. Diagram of $\varepsilon_{Nd(i)}$ *vs.* $(^{87}Sr/^{86}Sr)_i$ for whole-rock samples of the dykes as well as samples from the Ketilidian (Ket) and Archaean (Arch) basement. $(Th/Nb)_N$ ratios (normalized to primitive mantle values from McDonough and Sun, 1995) are given by small numbers attached to the symbols. The value for the initial $^{87}Sr/^{86}Sr$ ratio for bulk silicate Earth (BSE) is calculated using present-day ratios of $^{87}Sr/^{86}Sr$ = 0.745 and $^{87}Rb/^{86}Sr$ = 0.0827 (DePaolo, 1988). Additional data are given for comparison: EF: Eriksfjord Formation (Halama *et al.*, 2003); Iv: lamprophyres and basalts from the Ivittuut region (Goodenough *et al.*, 2002); Ku: gabbros from the Kûngnât ring dyke (Goodenough, unpublished); Gr(sy) and Gr(ca): syenites and carbonatites from the Grønnedal Ika intrusion (Halama *et al.*, 2005 (Nd data) and Taubald *et al.*, 2004 (Sr data)).



https://doi.org/10.1180/minmag.2015.079.4.04 Published online by Cambridge University Press

2002), gabbros from the Kûngnât ring-dyke (Goodenough, 1997) as well as syenites and carbonatites from the Grønnedal-Ika intrusion (Nd data from Halama *et al.*, 2005; Sr data from Taubald *et al.*, 2004). Two separate groups can be distinguished based on the isotopic characteristics. Lamprophyres and basalts from the Ivittuut region as well as carbonatites and syenites from the Grønnedal Ika intrusion have $\varepsilon_{Nd(i)}$ between 1.8 and 5.0 and $^{87}Sr/^{86}Sr_{(i)}$ values scattering around BSE. In comparison, gabbros from the Kûngnât complex as well as the lower lavas from the Eriksfjord Formation together with the BD of the present study have significantly lower $\varepsilon_{Nd(i)}$ between −0.1 and −4.4.

### *Geochemical classification of the individual swarms*

The BD are, on the basis of temporal relationships and orientation, divided into $BD_0$, $BD_1$ and $BD_2$. It is not evident from either the geochemical diagrams or any other respect that they represent three distinct suites. To test if the generations of BD can be fingerprinted, dykes that were emplaced into Archaean crust have been selected. This is assumed to minimize biases in incompatible element ratios between dykes emplaced in Archaean and Ketilidian basement. Based on Zr/Y and $La_N/Sm_N$ ratios, two geochemical groups can be identified: One hosting the majority of the $BD_0$ samples, and one the majority of $BD_1$ and $BD_2$ samples (Fig. 11). The increase in Zr/Y is related to the generally greater Zr contents in the $BD_0$ dykes (see positive Zr anomalies in Fig. 8) and the larger $(La/Sm)_N$ ratio reflects the steeper *LREE* spectrum for $BD_0$ dykes illustrated in Fig. 9. Although the geochemical grouping is broadly in accord with the cross-cutting relationships (Berthelsen and Henriksen, 1975), several exceptions are obvious. One $BD_0$ sample seems to be related to the geochemical group of $BD_1$ and $BD_2$ and five samples of $BD_1$ and $BD_2$ appear to be related to the $BD_0$ samples.

### *Tectonic environment*

The Gardar dykes have been emplaced in a continental rift-related environment. However, based on the Ta-Hf/3-Th diagram after Wood (1980) (Fig. 12), no clear classification as within-plate basalts (WPB) is possible. Instead, the

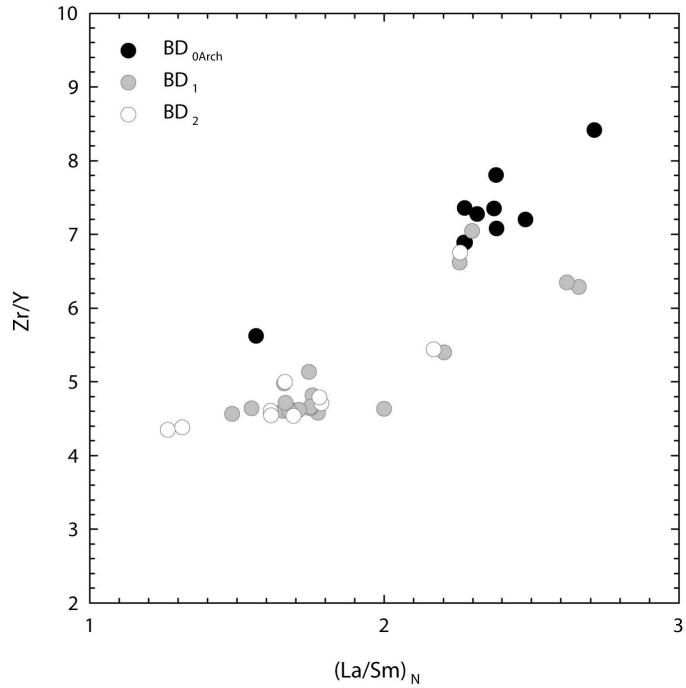


FIG. 11. Discrimination diagram for the individual dyke generations intruding Archaean basement using Zr/Y and $(La/Sm)_N$ whole-rock data. The concentrations of La and Sm are normalized to chondrite values from Boynton (1984).



https://doi.org/10.1180/minmag.2015.079.4.04 Published online by Cambridge University Press

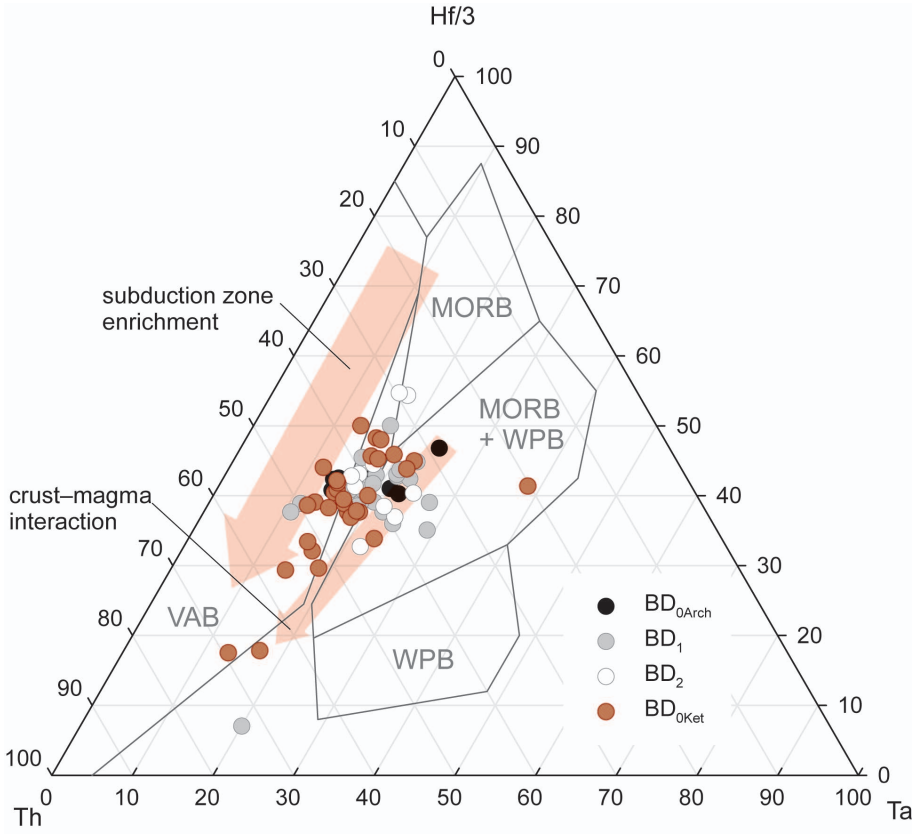


FIG. 12. Discrimination diagram for Ta-Hf-Th after Wood (1980) with fields indicated for possible tectonic settings: MORB = mid-ocean ridge basalts, WPB = within-plate basalts, VAB = volcanic arc basalts. Red arrows indicate subduction zone enrichment and crust-magma interaction, respectively.

majority of samples scatter between the field of enriched mid-ocean ridge basalts (MORB) and WPB and volcanic arc basalts (VAB). This could be related to modification of the used trace-element parameters during fractionation processes (Rollinson, 1993) or may indicate mantle source modification caused by subduction zone enrichment or crust-magma interaction as illustrated by the arrows given in Fig. 12 (Dudás, 1992; Pearce, 1996).

## Discussion

### *Fractional crystallization*

Minimum and maximum MgO values of 1.85 and 11.89 wt.% and calculated Mg# of 21.72–59.49 indicate a broad spectrum of compositions. However, the majority of the investigated samples have an MgO concentration and Mg# close to calculated median values of 6.14 wt.% and 45.25, respectively. These values suggest that the samples do not represent primary magmas, but originated from geochemically evolved melts and represent fractionated basalts with densities close to a minimum.

In general, an increasing abundance of *REE* with a slightly more pronounced *LREE* enrichment with decreasing Mg# (Fig. 9) is consistent with progressive crystallization from a differentiating melt (Blaxland and Upton, 1978). The major- and trace-element trends given in Fig. 6 and 7 can be used to identify fractional crystallization trends which governed the chemical evolution of the melts. In the following, the fractionating phases will be discussed in order of their typical appearance on the solidus.

The strong negative trend of Cr at large Mg# values indicates fractionation of Cr-spinel in the early evolution of melts or accumulation of chromite within the samples although no



https://doi.org/10.1180/minmag.2015.079.4.04 Published online by Cambridge University Press

accumulation is seen in the petrographic investigations. However, this trend is only observable for the oldest generation of dykes ($BD_0$). Significantly lower Cr concentrations (<100 ppm) for the most primitive samples of the younger dyke generations ($BD_1$ and $BD_2$) suggest that Cr-spinel had already fractionated from these melts during an earlier stage.

Fractionation of olivine is indicated by positive correlation of MgO, Co and Ni with Mg#. The low initial Ni and Co contents (<150 and <60 ppm, respectively) for the majority of the samples suggests additionally, that earlier fractionation of olivine influenced the melt evolution. Four outliers with low Co concentrations can be linked to marginal samples and possible contamination with basement rocks.

A slightly decreasing trend for Sr with decreasing Mg# can be observed for the $BD_{0Arch}$, $BD_1$ and $BD_2$. In contrast, samples of the $BD_{0Ket}$ dykes show a broad scatter of Sr against Mg# and a clear trend is absent. However, all dyke generations show positive Sr and Eu anomalies in the most primitive samples which decreases with increasing fractionation and turn into negative anomalies for the most fractionated samples (Figs 8 and 9). This indicates plagioclase accumulation during an earlier stage of melt evolution followed by normal fractional crystallization of plagioclase during dyke emplacement. The positive correlation of CaO and the negative correlation of $Na_2O$ with Mg# indicate that the fractionating plagioclase crystals were rich in anorthite. A possible source for early plagioclase accumulation could be related to the anorthositic bodies, which are assumed to underly the province as described by several authors (e.g. Bridgwater, 1967; Bridgwater and Harry, 1968; Upton *et al.*, 2003; Upton, 2013).

The majority of the samples display maximum values for Cr, Sc, V and Ca/Al between Mg# of 45–50 indicating the start of clinopyroxene fractionation in this range of Mg#. This is further supported by stronger decreasing trends of MgO and CaO as well as flattening of the curves for $Fe_2O_3$ and MnO below a Mg# of 45. Another indication for clinopyroxene fractionation is a positive correlation of Sc/Y and Mg# as suggested by Mattsson and Oskarsson (2005).

The curved trends for $TiO_2$, $Fe_2O_3$ and MnO with maximum values around Mg# ~35 and the strong decrease of Co and V below Mg# ~35 indicate fractionation of Fe-Ti-oxides in the late-stage of magma evolution. A negative correlation of Zn and Mg# suggests that the formation of magmatic ilmenite was negligible and the dominant Fe-Ti-oxide during fractionation was titanomagnetite. Accordingly, ilmenite crystals observed in the samples probably formed due to late-stage oxy-exsolution of primary titanomagnetite. It is only in the most evolved samples that fractionation of magmatic ilmenite might have occurred, as suggested by decreasing Zn concentrations. The fractionating mineral assemblage of plagioclase + olivine + augite + magnetite is consistent with the observed trend in the Zr/Ti *vs.* Nb/Y diagram (Fig. 4).

A decrease of $P_2O_5$, CaO and $\Sigma REE$ concentrations as well as Ca/Al ratios at low Mg# values (<35) give evidence for late-stage apatite fractionation. The decreasing contents of $K_2O$ less than Mg# of ~35 additionally indicate the formation of K-rich feldspar which has been fractionated from the melt. However, K-feldspar was not observed in thin sections of highly fractionated samples and possible K-feldspar components probably formed due to contamination with the K-rich basement. Most of the samples which deviate significantly from the above described trends can be attributed to marginal contamination.

### *Crustal contamination*

A complicating factor in a continental setting is the role of crustal contamination which often masks mantle source signatures and complicates petrogenetic interpretations. It can influence an initial melt composition at various stages during its evolution. Accordingly, mixing as well as assimilation accompanying fractional crystallization (AFC) processes may occur. In particular, at the margins of an intrusion, remobilization and partial melting of host rock could lead to progressive back-veining. This significantly changes the melt composition dependent on the composition of the host rock. In the following, the different possible crustal contamination processes are discussed, in an attempt to constrain the composition of primary melt(s) prior to reaction with crustal material.

Major-element compositions can be used as a first proxy to identify crustal contamination. Large $SiO_2$ and $K_2O$ (Fig. 6) concentrations at comparable primitive Mg# in some samples from the margins of dykes are taken as evidence for back-veining processes or host-rock interaction during the final emplacement of dykes. This is supported by field observations of granitic veins



https://doi.org/10.1180/minmag.2015.079.4.04 Published online by Cambridge University Press

in some of the dyke margins, representing remobilized basement rocks. A higher scatter in major and trace elements *vs.* Mg# is observed, especially in the wider $BD_0$ dykes and may be explained by a higher potential heat transfer at the margins of wider dykes and subsequent crustal contamination.

In order to provide further constraints on the contamination processes, AFC as well as mixing processes were modelled using the formulated spreadsheet from Ersoy and Helvaci (2010). Powell (1984) noted that a strong contrast in trace-element concentration between the sample and the contaminant is required before contamination can be recognized and in this study AFC processes were modelled using Th, U and La against Zr as a proxy for melt evolution. The starting composition in the models always represents the most primitive composition of the individual BD generations based on Mg# and mantle-normalized multi-element plots. The compositions of samples of Ketilidian and Archaean basement were used as contaminant. The percentage of fractionating minerals was chosen to represent a typical low-pressure assemblage, consisting of 50% plagioclase, 30% clinopyroxene and 20% olivine (Halama *et al.*, 2007). This is consistent with the mineral proportions observed in the samples of this study. However, even major changes in the fractionating mineral assemblage will not influence the results significantly due to the use of highly incompatible elements in the modelling. Different rates of assimilation to fractionation ($r$ = 0.1, 0.2 and 0.3) were tested in the calculation. The methodology used does not account for individual AFC processes which might have affected specific dykes, but gives an approximate value for the importance of crustal assimilation for a suite of dyke rocks.

The modelling indicates that crustal assimilation during crystal fractionation played only a minor role in the genesis of the BD, e.g. as exemplified in the Th *vs.* Zr plots (Fig. 13*a*–*d*). In most cases an assimilation rate <10% is indicated for the samples, although trends for La and U may

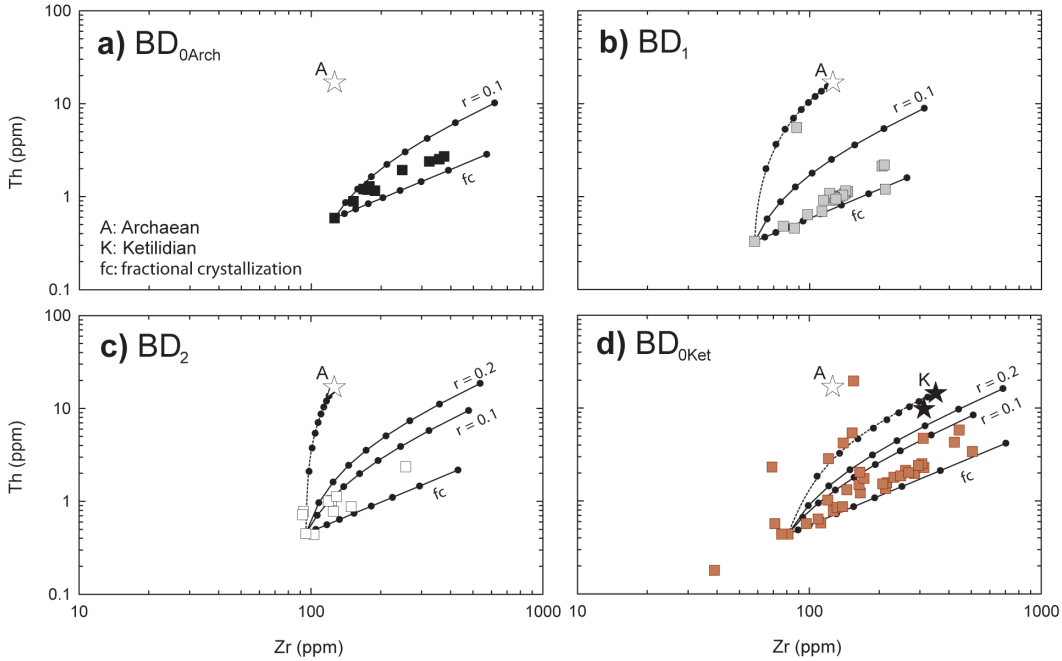


FIG. 13. Plots of Th *vs.* Zr for the individual dyke generation $BD_{0Arch}$ (*a*), $BD_1$ (*b*), $BD_2$ (*c*) and $BD_{0Ket}$ (*d*). fc: modelled trend for fractional crystallization; solid lines: modelled trends for assimilation during fractional crystallization (AFC) processes with $r$ = assimilation to fractionation rate. Modelling was conducted using Archaean (A) and Ketilidian (K) basement rock samples as contaminant and a fractionating mineral assemblage of 50% pl, 30% cpx and 20% ol; dashed lines: modelled mixing lines with Archaean (*b* and *c*) and Ketilidian (*d*) basement rocks.



https://doi.org/10.1180/minmag.2015.079.4.04 Published online by Cambridge University Press

suggest as much as 20%. Irrespectively, assimilation can effectively model the observed compositional trend of the investigated dykes. Binary mixing lines between dyke and basement rocks support the suggested contamination of some of the marginal dyke samples by back-veining and mixing processes (Fig. 13*b*–*d*). Some extreme outliers are thought to be related to local mineralogical or chemical heterogeneities of the contaminating basement rocks. A comparison of $(Th/Nb)_N$, used as an index for crustal contamination with increasing fractionation (decreasing Mg#) further supports the importance of AFC processes.

As even the most primitive parental melt sample is already evolved with regards to its MgO concentration (11.89 wt.%) and the majority of samples are in the range of ~6 wt.% MgO, crustal contamination during prior melt evolution has to be considered. In the Th/Yb *vs.* Nb/Yb diagram (Fig. 14, Pearce and Peate, 1995; Pearce, 2008), the majority of the samples plot in the range comparable to enriched mid-ocean ridge basalts (E-MORB) and describe a steep trend towards larger Th/Yb values. Following Pearce (2008), this indicates progressive melt-crust interaction due to selective enrichment of Th and is consistent with the modelled AFC processes as well as elevated $^{87}Sr/^{86}Sr_{(i)}$ and lowered $\varepsilon_{Nd(i)}$ values for samples with high $(Th/Nb)_N$ ratios (Fig. 10).

However, the typical features of HFSE depletion as well as enrichment of LILE and *LREE* can be observed even in the most primitive samples which plot within the mantle array in Fig. 14, defined by N-MORB, E-MORB and OIB compositions (Sun and McDonough, 1989). Therefore, it is considered that these melts were not significantly influenced by prior crustal contamination processes and developed their characteristic trace-element patterns before emplacement into the crust.

### *Assessment of secondary remobilization*

During weathering and metamorphism certain elements tend to be mobile, including the alkali

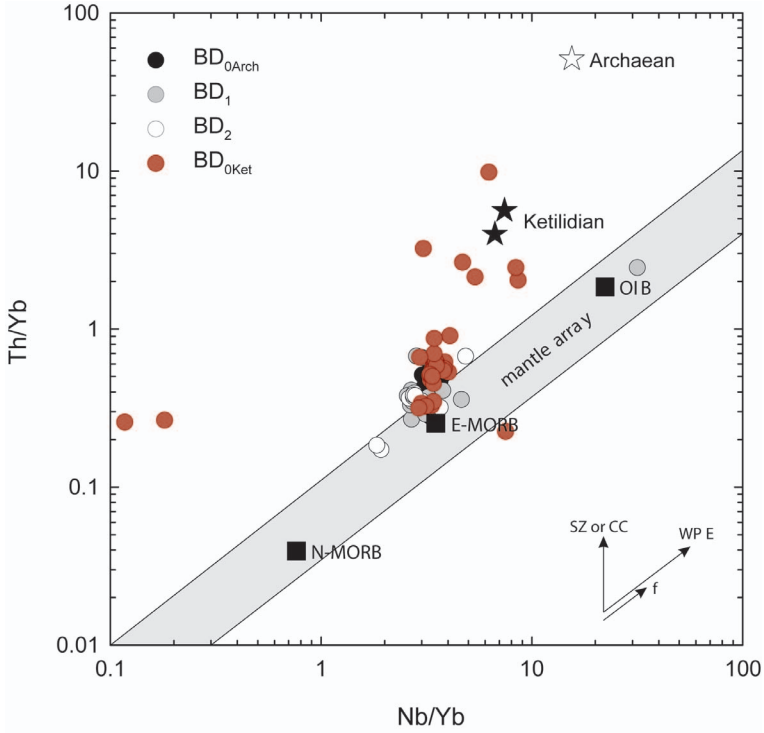


FIG. 14. Diagram of Th/Yb *vs.* Nb/Yb for whole-rock samples of the samples investigated. Normal mid-ocean ridge basalts (N-MORB), enriched mid-ocean ridge basalts (E-MORB) and ocean island basalt (OIB) values are taken from Sun and McDonough (1989). *SZ*: subduction zone enrichment; *CC*: crustal contamination; *WPE*: within-plate enrichment; *f*: fractional crystallization.



https://doi.org/10.1180/minmag.2015.079.4.04 Published online by Cambridge University Press

and alkali-earth metals (Pearce, 1996). As some samples show increased LOI values (electronic Table 2, deposited at www.minersoc.org/pages/e_journals/dep_mat_mm.html), taken as a first indication of secondary alteration, remobilization of elements is constrained before interpretation of the dataset using the approach given by Cann (1970). Good correlations of the possible mobile elements K, Ba, Sr and U with Zr, taken to be immobile during basalt fractionation, are evidence that these elements were not affected significantly by secondary alteration processes. In contrast, the concentrations of Cs and Rb in some of the samples do not show good correlation with Zr and should be considered carefully in the geochemical interpretation.

### Mantle sources

The geochemical data are used to constrain whether melts parental to the Gardar BD were generated in an upwelling plume, the sub-continental lithospheric mantle (SCLM), the sub-lithospheric upper mantle, or represent mixtures of these individual mantle components. In order to exclude the described effects of fractional crystallization and crustal contamination in the identification of these possible mantle sources, the dataset is restricted to samples with large Mg# (> 50) and low $(Th/Nb)_N$ ratios (< 1.6).

#### Plume origin

Involvement of a mantle plume within the younger period of Gardar magmatism is suggested by Halama *et al.* (2002, 2004 and 2007) and thus, should also be considered as a possible mantle source for the BD of the 'Older Gardar'. The HFSE contents and HFSE/HFSE ratios are useful tools to characterize the depletion and enrichment processes of the mantle source (McCulloch and Gamble, 1991; Pearce and Parkinson, 1993; Woodhead *et al.*, 1993; Pearce *et al.*, 2000; Pearce, 2008; Manikyamba *et al.*, 2009; Ray *et al.*, 2013). Niobium contents of 3–13 ppm and Zr/Nb ratios between 9–22, for the samples investigated, argue strongly against the influence of an enriched plume-related component in the generation of melts with geochemical characteristics comparable to modern OIB with Nb contents of 45 ppm and Zr/Nb ratios of ~6 (Sun and McDonough, 1989). In contrast, they indicate an only mildly-enriched source with a composition comparable to Archaean upper mantle (Polat and Kerrich, 1999 and 2002; Wyman *et al.*, 1999; Hollings and Kerrich, 2004 and 2006; Polat and Munker, 2004; Manikyamba *et al.*, 2009 and Wyman and Kerrich, 2009). A plume scenario is further unrealistic, assuming that the depth of melting was shallower than the garnet stability field. This is indicated by $(Gd/Yb)_N$ and $(Sm/Yb)_N$ ratios between 1.4–1.9 and 1.6–3.2 combined with almost constant chondrite-normalized *HREE* concentrations from Ho to Lu (Rollinson, 1993).

#### Evidence for a major SCLM component

Characteristic negative Hf anomalies as shown in Fig. 8 as well as similar Nb/Ta (13–29) and slightly higher Zr/Hf (37–51) ratios relative to MORB values of 18 and 36 (Sun and McDonough, 1989), suggest the presence of residual amphibole in the source (Moine *et al.*, 2001). This could be related to hydrous metasomatism and fertilization of a depleted source caused by, e.g. a preceding subduction event (Munker *et al.*, 2004; Davidson *et al.*, 2007; Manikyamba *et al.*, 2009) which is consistent with the observed enrichment of LILE and *LREE* (Figs 8 and 9). However, Köhler *et al.* (2009) proposed that the metasomatism introduced fluor-apatite and fluor-phlogopite into the SCLM, which could equally account for the raised LILE and *LREE*. Considering subduction-induced metasomatism, Th and *REE* systematics as well as the comparison of Ba/La and Th/Yb ratios are useful tools to further discriminate between metasomatism caused either by fluid or sedimentary input (Hawkesworth *et al.*, 1997; Woodhead *et al.*, 2001). The Th/Ce ratios of mantle derived rocks are typically in the range of 0.016–0.050 (average of MORB and OIB, Sun and McDonough, 1989) but they are much higher in sediments with a continental crust component. In an arc setting, Th appears to be preferentially mobilized from the sedimentary component (Pearce, 2008; Hawkesworth *et al.*, 1997) and any input from sediments would significantly increase the Th/Ce ratio. However, measured ratios of 0.021–0.035 ($m$ = 0.026), together with small total Th contents (0.33–1.21, $m$ = 0.64 ppm) indicate a fluid-dominated metasomatism of the mantle source. The wide range of Ba/La (18–30) ratios at relatively constant Th/Yb ratios (0.2–0.5) strengthens the case for the magmas being derived from a previously depleted source, subsequently enriched by fluids.

Light-*REE* systematics can be used for the identification of possible source heterogeneities or



https://doi.org/10.1180/minmag.2015.079.4.04 Published online by Cambridge University Press

different degrees of partial melting in the source region. In a La/Sm *vs*. Nb/La plot, a positive correlation would be consistent with different degrees of partial melting from a homogeneous mantle source. This is attributed to the decreasing incompatibility from Nb to La to Sm (Ray *et al.*, 2013). Accordingly, high La/Sm and Nb/La ratios represent the lowest degree of partial melting. However, since no positive trend is observable in Fig. 15, the differences in the La/Sm ratios are more likely to be attributed to a heterogeneous source or to variable degrees of mixing of a melt from a primitive asthenospheric upper mantle and melts from a metasomatized SCLM component (see discussion below).

The combination of constraints from the trace element concentrations and ratios provide strong evidence for the involvement of a major SCLM component in the generation of melts and the following possible scenarios are suggested: (1) mixing or assimilation of melts from primitive asthenospheric upper mantle with a SCLM component; (2) direct melting of the SCLM which had previously experienced extensive melt extraction and subsequent fertilization by fluids; or (3) significant crustal assimilation of melts from the asthenospheric mantle. As discussed above, crustal contamination was generally negligible and accordingly the third scenario cannot account for the trace-element characteristics observed for the data. Consequently, a strong contribution of a SCLM component in the evolution of the BD parental magmas is suggested. This component could have been the SCLM that had been modified by fluids from a subducting oceanic slab dating back to the Palaeo-Proterozoic Ketilidian orogeny (Garde *et al.*, 2002; Goodenough *et al.*, 2002; Upton, 2013). To account for the high Al/Ca ratios of the Gardar basic rocks throughout the Province, inferred to have been a primitive characteristic acquired during mantle melting, the latter was inferred to have originally had a depleted, possibly harzburgitic composition with low clinopyroxeme/garnet or clinopyroxene/spinel content. Metasomatism introduced LILE as well as inferentially F and Cl rendering the refractory SCLM fusible (Upton and Emeleus, 1987). Since the Ketilidian orogeny, the Gardar region remained stable and unaffected by tectonic or magmatic activity and the subduction-related signature was most likely preserved in the source regions of the Gardar magmas (Goodenough *et al.*, 2002). Indications for a veined SCLM are given by the occurrence of small mela-aillikitic intrusions (Upton *et al.*, 2006) and veined peridotitic mantle xenoliths (Upton, 1991) of Gardar age.

### *Sub-lithospheric or lithospheric sources*

Two remaining scenarios are envisaged for the formation of the BD magmas. The first is based on the assumption that the lithospheric mantle was characterized by abundant veins, rich in clinopyroxene, phlogopite and amphibole which could

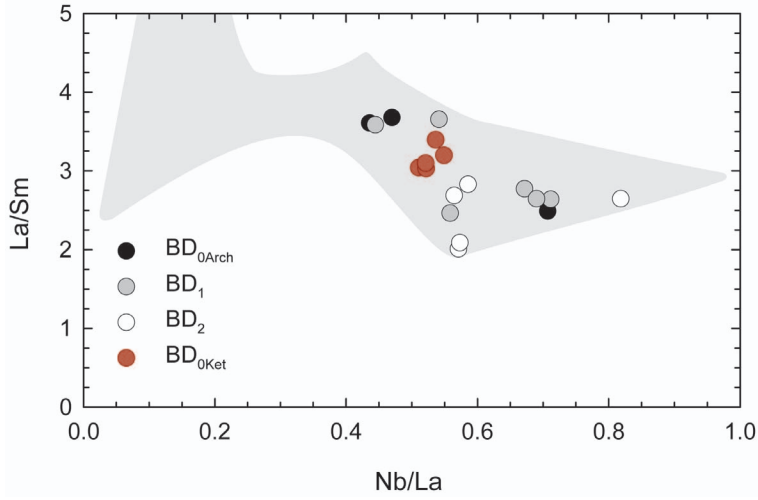


FIG. 15. Whole-rock La/Sm *vs.* Nb/La plot for samples with large Mg# (>50) and low $(Th/Nb)_N$ ratios (<1.6). The grey field illustrates the compositional range of the complete sample set of dyke rocks investigated.



https://doi.org/10.1180/minmag.2015.079.4.04 Published online by Cambridge University Press

be melted readily and the resultant melts intermixed with uprising asthenospheric upper mantle magmas. Cadman *et al.* (1995) successfully modelled the enrichment of Rb, Ba and K in Proterozoic dykes from Labrador, using the composition of N-type MORB asthenospheric material and veined xenoliths from metasomatized peridotites (O'Reilly *et al.*, 1991). Although this model could explain the enriched LILE characteristics observed in the rocks of the present study, it does not explain the observed enrichment of *LREE* in the samples studied. Luttinen *et al.*, (1998) and Luttinen and Furnes (2000) suggested a composition close to lamproites as a hypothetical composition for enriched veins in the SCLM. Following their approach, different lamproitic compositions (Rock, 1991; Cullers and Berendsen, 2011) have been tested in a mixing model with an N-MORB component from Sun and McDonough (1989) taken as reference material for primitive asthenospheric upper mantle melts. A mixing model between N-MORB and 5–10% lamproitic component give the best results for the dataset of the present study (Fig. 16). However, some characteristics of the samples argue against such a model. In particular, the *HREE* concentrations deviate significantly from the modelled composition and an unrealistic high degree of mixing with vein-melt would be necessary to explain the *HREE* systematics with the proposed model.

The second scenario envisaged is direct melt generation within the lithospheric mantle. The probable presence of amphibole or fluor-phlogopite + fluorapatite (Köhler *et al.*, 2009) supports a source restricted to the lithospheric mantle rather than a derivation from sub-lithospheric primitive upper mantle intermixed with lithospheric mantle components. This is supported by La/Ba *vs.* La/Nb systematic of the BD (Fig. 17) which shows significant overlap with the low-Ti Karoo basalts, the Umkondo low-Ti dykes as well as the Sudbury dykes each of which have also been attributed to a metasomatized lithospheric mantle source (Jourdan *et al.*, 2007, 2009; Shellnutt and MacRae, 2012).

The general isotopic variation of the early Gardar magmatic rocks (Fig. 10) may indicate a broadly similar but heterogeneous SCLM source, affected by variable degrees of metasomatism as proposed formerly by Goodenough *et al.* (2002) and Upton *et al.* (2003). However, the available data, especially those for the lamprophyric and basaltic dykes in the Grønnedal-Ika and Ivittuut regions that have higher $\varepsilon_{Nd(i)}$, provide evidence for a different, more primitive source. One

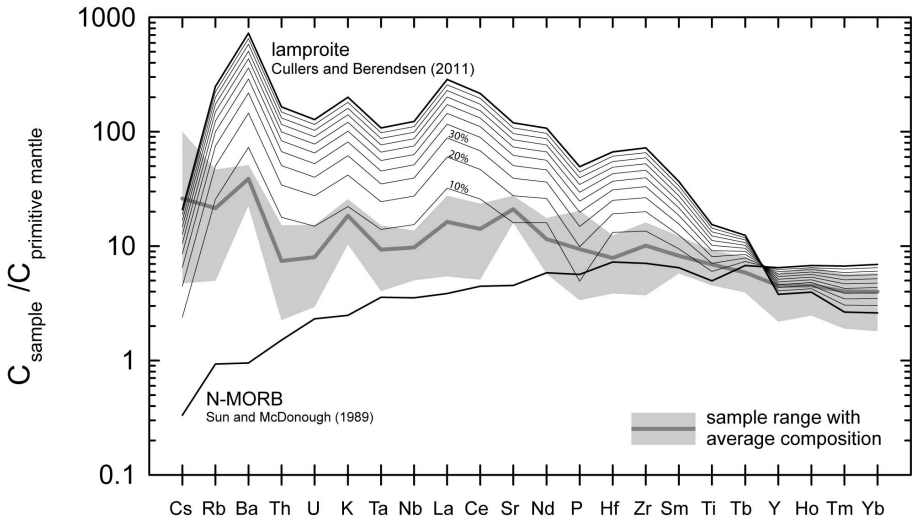


FIG. 16. Multi-element plot of incompatible trace elements normalized to primitive mantle values from McDonough and Sun (1995). Compositional range (grey field) and average composition (grey solid line) for whole rock samples of the dykes investigated with large Mg# (>50) and low $(Th/Nb)_N$ ratios (<1.6) are shown. Black solid lines illustrate a mixing model between N-MORB (Sun and McDonough, 1989) and lamproite (Cullers and Berendsen, 2011, average of 89 shallow samples from Silver City) composition. The interval for the mixing model is given in 10% steps.



https://doi.org/10.1180/minmag.2015.079.4.04 Published online by Cambridge University Press

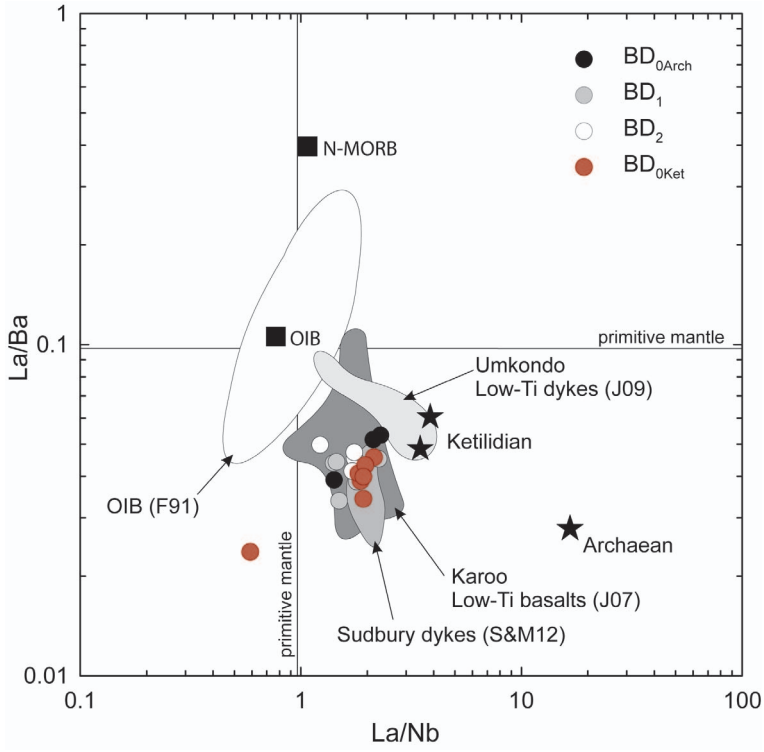


FIG. 17. Whole-rock La/Ba *vs.* La/Nb plot for samples with large Mg# (>50) and low $(Th/Nb)_N$ ratios (<1.6) as well as for samples from Archaean and Ketilidian basement. Additional data given for comparison are taken from: J07 = Jourdan *et al.* (2007), J09 = Jourdan *et al.* (2009), SandM12 = Shellnutt and MacRae (2012), F91 = Fitton *et al.* (1991). N-MORB, OIB and primitive mantle values are taken from Sun and McDonough (1989).

explanation is given by Goodenough *et al.* (2002) who interpreted the lamprophyres in the Ivittuut area as small-degree melts of an asthenospheric source which became frozen in as metasomatites in the SCLM during initiation of the Gardar rift and re-melted easily during rifting. This is also supported by their Pb isotope systematics which are substantially different from those of other Gardar basic rocks (Upton *et al*., 2003). Another possibility could be related to modifications of the isotopic signature by fluids associated with the emplacement of the Ivigtut and Grønnedal-Ika intrusions. However, it has to be mentioned that both scenarios are highly speculative and remain to be tested in future investigations.

### *Evolution of the early Gardar plumbing system*

The overall geochemical characteristics of the BD within the Gardar Province can be explained by postulating large deep crustal magma chambers underplated near the crust-mantle boundary in which magma was stored long enough to efficiently homogenize. This is consistent with the consensus view that the Older Gardar syenitic magmas within the Grønnedal-Ika, Kûngnât, Motzfeldt and North Qôroq complexes were largely fractional crystallization products from basaltic parents. Accordingly their genesis certainly required large volumes of the parental magmas many times their collective volumes. The evolved character of the melts in the dykes was probably caused by previous loss of olivine and Cr-rich spinel. Progressive crustal thinning during back-arc basin induced rifting (see discussion below) resulted in opening magma conduits and the formation of smaller magma chambers in which further fractional crystallization and assimilation processes took place. Thereby, the individual dyke generations ($BD_0$, $BD_1$ and $BD_2$) experienced very similar crystallization histories.



https://doi.org/10.1180/minmag.2015.079.4.04 Published online by Cambridge University Press

However, distinctive trace-element characteristics of the oldest $BD_0$ dyke generation when compared to those of the $BD_1$ and $BD_2$ dykes indicate a heterogeneous source region as proposed by Köhler *et al.* (2009). Additionally, the general, more enriched character of the first $BD_0$ generation, indicates a greater degree of fractional crystallization prior to emplacement.

### *Dyke swarm correlation and Mesoproterozoic rifting*

The magmatism in the Gardar Province can be correlated to near-contemporaneous and transatlantic dyke emplacement. During the Mesoproterozoic, the Columbia supercontinent was affected by numerous rift-related tectonomagmatic events involving the emplacement of mafic dykes, sills and the eruption of volcanic rocks. Most of the major events, including the world's largest radiating dyke swarm, the 1270 Ma Mackenzie swarm, have been linked to mantle plume activity and the separation of Siberia from the supercontinent (Evans and Mitchell, 2011 and references therein). However, the relationships between several dyke swarms (Sudbury, Mealy, Harp, Nain, Gardar) emplaced between 1235 and 1290 Ma (Cadman *et al.*, 1993; Buchan *et al.*, 1996; Hamilton *et al.*, 2010; Shellnutt and MacRae, 2012; Upton, 2013) within a corridor from southeastern Ontario to southwest Greenland, are still a matter of debate.

Recent geochemical and geochronological data from mafic dykes within the Timmiarmiit area in South East Greenland (Bartels *et al.*, 2014) show that early Gardar magmatism was far more widespread than previously thought. In addition, the geochemical characteristics, as well as the geochronological record of the Gardar BD and the Timmiarmiit dykes, are very similar to those of the dyke swarms located in the above mentioned corridor in central to eastern Canada (Fig. 18). The Nain and Harp dyke swarms in Labrador were investigated by Buchan *et al.* (1996) and Hamilton *et al.* (2010) who proposed a possible link to the Older Gardar intrusions. On the basis of whole-rock and mineral geochemistry, the suggestion that the Sudbury dykes were not directly related to mantle plume activity but to melts from a mantle source that had been modified by a subduction event (Shellnutt and MacRae, 2012), is consistent with the proposed formation of the Gardar BD and also accords with previous conclusions relating to Gardar basic magmas in general (Goodenough *et al.*, 2002; Upton *et al.* 2003). In the 1270 Ma plate reconstruction model (Evans and Mitchell, 2011), the above-mentioned pene-contemporaneous magmatic provinces occur behind a long-lived

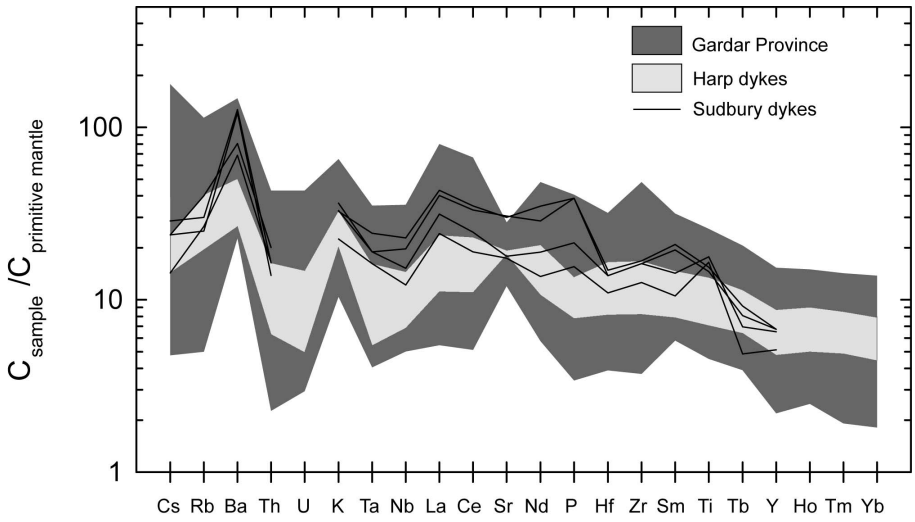


FIG. 18. Primitive mantle normalized multi-element pattern of incompatible elements comparing the geochemical characteristics of whole-rock samples of the dyke rocks investigated from the Gardar Igneous Province, South Greenland, with dykes in Labrador (Harp: data provided by Jean Goutier from the Quebec Geological Survey) and Central Canada (Sudbury: data from Shellnutt and MacRae, 2012 (SandM12)). Normalizing factors are taken from McDonough and Sun (1995)



https://doi.org/10.1180/minmag.2015.079.4.04 Published online by Cambridge University Press

accretionary margin wrapped around the southern margin of the Columbia supercontinent (Fig. 19) (Karlstrom *et al.*, 2001). The reconstruction also suggests the possibility that the Central Scandinavian Dolerite Group (CSDG) emplaced between 1290 to 1240 Ma (compilation from Brander *et al.*, 2011) represents an extension of the North American and South Greenlandic magmatism. Based on geochronological and Lu-Hf isotopic data, Söderlund *et al.* (2006) suggested that the CSDG could be explained by prolonged hotspot activity or, alternatively, by discrete extensional events in a back-arc setting behind an active continental margin to the west.

From the available geochemical and geochronological data as well as plate reconstructions (Evans and Mitchell, 2011; Johansson, 2013), a petrogenetic link between the Sudbury, Nain, Harp, Timmiarmiit dykes and the CSDG intrusions with the Older Gardar BD is hypothesized. Following the alternative suggestion of Söderlund *et al.* (2006), it is suggested that the above mentioned dyke swarms formed behind a long-lived orogenic belt in response to back-arc basin formation between 1290–1235 Ma. Direct evidence for the accretionary orogeny during this time is lacking in South Greenland, but comes from the Grenville Province of southern Labrador and eastern Quebec where several arc-related terranes amalgamated against the south-eastern Laurentian margin during the Elzevirian orogeny between 1300 and 1200 Ma (Moore and Thompson, 1980). This amalgamation culminated in the so-called Grenvillian orogeny (Rivers, 1997) from 1200 to 980 Ma. Equivalents of these accretionary processes can also be traced in southern Scandinavia where they are linked to the Sveconorwegian (Grenvillian) orogeny (Karlstrom *et al.* (2001).

## Conclusion

The comprehensive geochemical dataset presented here, including a wide range of HFSE, enables precise determination of fractional crystallization as well as crustal contamination processes and thus allows characterization of the mantle melt composition, parental to the Gardar

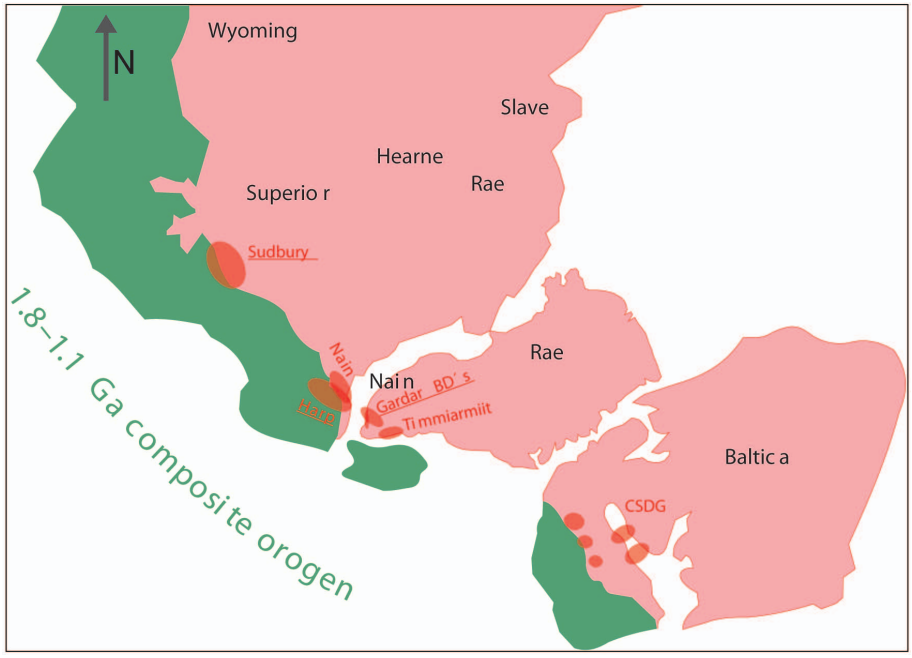


FIG. 19. Plate reconstruction of the Columbia super-continent at 1270 Ma, modified after Evans and Mitchell (2011). Indicated are names of cratons (black) and mafic dyke swarms emplaced between 1235–1290 Ma (red). The sample localities for the geochemical data shown in Fig. 18 are indicated by underlined locality names. CSDG: Central Scandinavian Dolerite Group.



https://doi.org/10.1180/minmag.2015.079.4.04 Published online by Cambridge University Press

BD. This melt composition was influenced by a major SCLM component as also proposed by previous studies (Upton and Emeleus, 1987; Upton *et al.*, 2003; Köhler *et al.*, 2009; Upton, 2013). This component developed during the Ketilidian orogeny ~500 Ma years prior to the genesis of the BD, where intensive magmatism left a depleted underlying mantle which was contemporaneously metasomatized by fluids from the subducting plate.

The detailed geochemical data of the present study also allows a comparison and correlation of the geochemical fingerprint of the early Gardar BD to pene-contemporaneous dyke swarms in North America and Central Scandinavia. Together with recent plate reconstruction models (Evans and Mitchell, 2011; Johansson, 2013), these correlations give strong evidence for a petrogentic link between the different dyke swarms and their generation in response to back-arc basin formation in the time interval between 1235–1290 Ma.

## Acknowledgements

The authors acknowledge the pioneering work of C.E. Wegmann who first described the occurrence of the 'brown dykes' within the Gardar Province. This manuscript benefited greatly from the reviews of Kathryn M. Goodenough, Jean Bédard and an anonymous reviewer. Asger Ken Pedersen and Zina Fihl provided and helped to find archive sample material from the University of Copenhagen. Stuart Watt and Lotte Melchior Larsen helped with sample maps, field diaries and data from the GEUS archive. Michael Marks and Gregor Markl are thanked for providing sample material from the University of Tübingen. The authors thank Per Kalvig, Henning Bohse and Thomas Ulrich for their organization, assistance and help during field work. The interpretation of the data benefited from fruitful discussions with Thomas Find Kokfelt and Jakob Kløve Keiding. The assistance of Michael Nielsen with the preparation of samples is acknowledged.

## References

Allaart, J.H. (1969). *The chronology and petrography of the Gardar dykes between Igaliko Fjord and Redekammen, South Greenland*. Rapport Grønlands Geologiske Undersøgelse, **25**. GEUS, Copenhagen, 26 pp.

Arndt, N.T. and Christensen, U. (1992) The role of lithospheric mantle in continental flood volcanism: Thermal and geochemical constraints. *Journal of Geophysical Research*, **97**, 10967–10981.

Ayrton, S.N. (1963) *A contribution to the geological investigations in the region of Ivigtut, S. W. Greenland*. Meddelelser om Grønland, **167**. GEUS, Copenhagen, 139 pp.

Bartels, A., Nilsson, M.K.M., Klausen, M.B. and Söderlund, U. (2014) The Gardar Igneous Province, South-East Greenland. South-East Greenland Workshop 2014, Abstract volume. *Danmarks og Grønlands Geologiske Undersøgelse Rapport* (in press).

Berthelsen, A. (1958) Geological map of the Ivigtut peninsula, 1:20000. In: *Geological map of Greenland 1:100 000. Ivittuut 61 V.1 Syd* (A. Berthelsen and N. Henriksen, 1975) Geological Survey of Greenland, Copenhagen.

Berthelsen, A. and Henriksen, N. (1975) *Geological map of Greenland, 1:100 000, Ivigtut 61 V. 1 syd. Descriptive text*. Geological Survey of Greenland, Copenhagen [also Meddelelser om Grønland **186**.**1**].

Blaxland, A.B. and Upton, B.G.J. (1978) Rare-earth distribution in the Tugtutôq younger giant dyke complex: evidence bearing on alkaline magma genesis in South Greenland. *Lithos*, **11**, 288–299.

Bondesen, E. (1957) *Field map with indicated geological observations*. GEUS map archive: 61 V.1 100. GEUS, Copenhagen.

Bondesen, E. (1958) *Field map with indicated geological observations*. GEUS map archive: 61 V.1 125. GEUS, Copenhagen.

Boynton, W.V. (1984) Geochemistry of the rare earth elements: meteorite studies. Pp. 63–114 in: *Rare Earth Element Geochemistry* (P. Hendersen, editor). Elsevier, Amsterdam.

Brander, L., Söderlund, U. and Bingen, B. (2011) Tracing the 1271–1246 Ma Central Scandinavian Dolerite Group mafic magmatism in Fennoscandia: U–Pb baddeleyite and Hf isotope data on the Moslätt and Børgefjell dolerites. *Geological Magazine*, **148**, 632–643.

Bridgwater, D. (1967) Feldspathic inclusions in the Gardar igneous rocks and their relevance to the formation of major anorthosites in the Canadian shield. *Canadian Journal of Earth Sciences*, **4**, 995–1014.

Bridgwater, D. and Harry, W.T. (1968) *Anorthosite xenoliths and plagioclase megacrysts in Precambrian intrusions of South Greenland*. Bulletin Grønlands Geologiske Undersøgelse, **77**. GEUS, Copenhagen, 243pp [also Meddelelser om Grønland, **185**].

Buchan, K.L., Hodych, J.P., Roddick, J.C., Emslie, R.F. and Hamilton, M.A. (1996) Paleomagnetism and U-Pb geochronology of Mesoproterozoic dykes of Labrador and correlations with dykes of southwest



https://doi.org/10.1180/minmag.2015.079.4.04 Published online by Cambridge University Press

Greenland. Abstract p. 37 in: *Proterozoic Evolution in the North Atlantic Realm*. Program and Abstracts, International conference IGCP Project 371 (Compiled by C.F. Gower). COPENA–ECSOOT–IBTA conference, Goose Bay, Labrador, Canada.

Cadman, A.C., Heaman, L.M., Tarney, J., Wardle, R.J. and Krogh, T.E. (1993) U-Pb geochronology and geochemical variation within two Proterozoic mafic dyke swarms, Labrador. *Canadian Journal of Earth Sciences*, **30**, 1490–1504.

Cadman, A.D., Tarney, J. and Baragar, W.R.A. (1995) Nature of mantle source contributions and the role of contamination and in situ crystallisation in the petrogenesis of Proterozoic mafic dykes and flood basalts Labrador. *Contributions to Mineralogy and Petrology*, **122**, 2013–229.

Cann, J.R. (1970) Rb, Sr, Y, Zr and Nb in some ocean floor basaltic rocks. *Earth and Planetary Science Letters*, **10**, 7–11.

Coulson, I.M., Goodenough, K.M., Pearce, N.J.G. and Leng, M.J. (2003) Carbonatites and lamprophyres of the Gardar Province – a 'window' to the sub-Gardar mantle? *Mineralogical Magazine*, **67**, 855–872.

Cullers, R.L. and Berendsen, P. (2011) *Mineralogical and Chemical Evolution of Lamproites in Woodson and Wilson Counties, Southeastern Kansas*. New Technical Series, **22**. Kansas Geological Survey, Kansas, USA.

Davidson, J., Turner, S. and Handley, H. (2007) Amphibole "sponge" in arc crust? *Geology*, **35**, 787–790.

DePaolo, D.J. (1988) *Neodymium Isotope Geochemistry: An Introduction*. Springer-Verlag, New York.

Dudás, F.O. (1992) Petrogenetic evaluation of trace element discrimination diagrams. Pp. 93–127 in: *Basement Tectonics 8* (M.J. Batholomew, D.W. Hyndman, D.W. Mogk and R. Mason, editors). Kluwer, Dordrecht, The Netherlands.

Ersoy, Y. and Helvaci, C. (2010) FC–AFC–FCA and mixing modeler: A Microsoft® Excel spreadsheet program for modelling geochemical differentiation of magma by crystal fractionation, crustal assimilation and mixing. *Computers and Geosciences*, **36**, 383–390.

Evans, D.A.D. and Mitchell, R.N. (2011) Assembly and breakup of the core of Paleoproterozoic–Mesoproterozoic supercontinent Nuna. *Geology*, **39**, 443–446.

Fitton, J.D., James, D., Leeman, W.P. (1991) Basic magmatism associated with late Cenozoic extension in the Western United States: compositional variations in space and time. *Journal of Geophysical Research*, **96**, 13693–13711.

Gallagher, K. and Hawkesworth, C. (1992) Dehydration melting and the generation of continental flood basalts. *Nature*, **258 (1992)**, 57–59.

Garde, A.A., Hamilton, M.A., Chadwick, B., Grocott, J. and McCaffrey, K.J.W. (2002) The Ketilidian orogen of South Greenland: geochronology, tectonics, magmatism and fore-arc accretion during Palaeoproterozoic oblique convergence. *Canadian Journal of Earth Sciences*, **39**, 765–793.

Goldstein, S.L., O'Nions, R.K. and Hamilton, P.J. (1984) A Sm–Nd isotopic study of the atmospheric dust and particulates from major river systems. *Earth and Planetary Science Letters*, **70**, 221–236.

Goodenough, K.M. (1997) *Geochemistry of Gardar intrusions in the Ivittuut area, South Greenland*. PhD thesis, Edinburgh University, Edinburgh, UK.

Goodenough, K.M., Upton, B.G.J. and Ellam, R.M. (2002) Long-term memory of subduction processes in the lithospheric mantle. Evidence from the geochemistry of basic dykes in the Gardar Province of South Greenland. *Journal of the Geological Society (London)*, **159**, 1–10.

Halama, R., Waight, T. and Markl, G. (2002) Geochemical and isotopic zoning patterns of plagioclase megacrysts in gabbroic dykes from the Gardar Province, South Greenland: implications for crystallisation processes in anorthositic magmas. *Contributions to Mineralogy and Petrology*, 144, 109–127.

Halama, R., Wenzel, T., Upton, B.G.J., Siebel, W. and Markl, G. (2003) A geochemical and Sr-Nd-O isotopic study of the Proterozoic Eriksfjord Basalts, Gardar Province, South Greenland: Reconstruction of an OIB signature in crustally contaminated rift-related basalts. *Mineralogical Magazine*, **67**, 831–853.

Halama, R., Marks, M., Brügmann, G., Siebel, W., Wenzel, T. and Markl, G. (2004) Crustal contamination of mafic magmas: evidence from a petrological and Sr-Nd-Os-O isotopic study of the Proterozoic Isortoq dike swarm, South Greenland. *Lithos*, **74**, 199–232.

Halama, R., Vennemann, T., Siebel, W. and Markl, G. (2005) The Grønnedal-Ika carbonatite–syenite complex, South Greenland: Carbonatite formation by liquid immiscibility. *Journal of Petrology*, **46**, 191–217.

Halama, R., Joron, J.-L., Villemant, B., Markl, G. and Treuil, M., (2007) Trace element constraints on mantle sources during mid-Proterozoic magmatism: evidence for a link between the Gardar (South Greenland) and Abitibi (Canadian Shield) mafic rocks. *Canadian Journal of Earth Sciences*, **44**, 459–478.

Hamilton, M.A., Buchan, K.L. and Hodych, J.P. (2010) Nain/Gardar-aged mafic dykes as a temporal and magmatic 'bridge' across North Atlantic cratonic blocks: geochronologic, paleomagnetic and



https://doi.org/10.1180/minmag.2015.079.4.04 Published online by Cambridge University Press

geochemical evidence from Labrador and SW Greenland. Conference abstract, *6th International Dyke Conference*, Varanasi, India, Third and Final Circular, IDC-6 abstracts.

Hawkesworth, C. J., Turner, S.P., McDermott, F., Peate, D.W. and van Calsteren, P. (1997) U–Th isotopes in arc magmas: implications for element transfer from the subducted crust. *Science*, **276**, 551–555.

Hollings, P. and Kerrich, R. (2004) Geochemical systematics of tholeiites from the 2.86 Ga pickle crow assemblage, northwestern Ontario: arc basalts with positive and negative Nb–Hf anomalies. *Precambrian Research*, **134**, 1–20.

Hollings, P. and Kerrich, R. (2006) Light rare earth element depleted to enriched basaltic flows from 2.8 to 2.7 Ga greenstone belts of the Uchi subprovince, Ontario, Canada. *Chemical Geology*, **227**, 133–153.

Irvine, T.N. and Baragar, W.R.A. (1971) A guide to the chemical classification of the common volcanic rocks. *Canadian Journal of Earth Science*, **8**, 523–548.

Jacobson, S.B. and Wasserburg, G.J. (1980) Sm–Nd isotopic evolution of chondrites. *Earth and Planetary Science Letters*, **50**, 139–155.

Johansson, A. (2013) From Rodinia to Gondwana with the 'SAMBA' model – A distant view from Baltic towards Amazonia and beyond. *Precambrian Research*, **244**, 226–235.

Jordan, T.H. (1988) Structure and formation of the continental tectosphere. Special Issue: Oceanic and continental lithosphere: Similarities and differences. *Journal of Petrology*, **Special Volume 1**, 11–37.

Jourdan, F., Bertrand, H., Sharer, U., Blichert-Toft, J., Féraud, G. and Kampunzu, A.B. (2007) Major and trace element and Sr, Nd, Hf, and Pb isotope compositions of the Karoo large igneous province, Botswana–Zimbabwe: lithosphere *vs* mantle plume contribution. *Journal of Petrology*, **48**, 1043–1077.

Jourdan, F., Bertrand, H., Féraud, G., Le Gall, B. and Watkeys, M.K. (2009) Lithospheric mantle evolution monitored by overlapping large igneous provinces: Case study in southern Africa. *Lithos*, **107**, 257–268.

Karlstrom, K.E., Åhäll, K.-I., Harlan, S.S., Williams, M.L., McLelland, J. and Geissman, J.W. (2001) Long-lived (1.8–1.0 Ga) convergent orogen in southern Laurentia, its extensions to Australia and Baltica, and implications for refining Rodinia. *Precambrian Research*, **111**, 5–30.

Köhler, J., Schönenberger, J., Upton, B.G.J. and Markl, G. (2009) Halogen and trace element geochemistry in the magmatic Gardar Province, South Greenland: evidence for subduction-related mantle metasomatism and fluid exsolution processes from alkaline melts. *Lithos*, **113**, 731–747.

Kretz, R. (1983) Symbols for rock-forming minerals. *American Mineralogist*, **68**, 277–279.

Luttinen, A.V. and Furnes H. (2000) Flood Basalts of Vestfjella: Jurassic Magmatism Across an Archaean–Proterozoic Lithospheric Boundary in Dronning Maud Land, Antarctica. *Journal of Petrology*, **41**, 1271–1305.

Luttinen, A.V., Rämö, O.T. and Huhma, H. (1998) Nd and Sr isotopic and trace element composition of a Mesozoic CFB suite from Dronning Maud Land, Antarctica: implications for lithosphere and asthenosphere contributions to Karoo magmatism. *Geochimica et Cosmochimica Acta*, **62**, 2701–2714.

Manikyamba, C., Kerrich, R., Khanna, T.C., Satyanarayanan, M. and Krishna, A.K. (2009) Enriched and depleted arc basalts, with Mg-andesites and adakites: a potential paired arc- back-arc of the 2.6 Ga Hutti greenstone terrane, India. *Geochimica et Cosmochimica Acta*, **73**, 1711–1736.

Mattsson, H.B. and Oskarsson, N. (2005) Petrogenesis of alkaline basalts at the tip of a propagating rift: evidence from the Heimaey volcanic centre, south Iceland. *Journal of Volcanology and Geothermal Research*, **147**, 245–267.

McCulloh, M.T. and Gamble, A.J. (1991) Geochemical and geodynamical constraints on subduction zone magmatism. *Earth Planetary and Science Letters*, **102**, 358–374.

McDonough, W.F.M. and Sun, S.S. (1995) The composition of the Earth. *Chemical Geology*, **120**, 223–253.

Moine, B.N., Grégoire, M., O'Reilly, S.Y., Sheppard, S.M. and Cottin, J.-Y. (2001) High Field Strength Element Fractionation in the Upper Mantle: evidence from amphibole-rich composite mantle xenoliths from the Kerguelen Islands (Indian Ocean) *Journal of Petrology*, **42**, 2145–2167.

Moore, J.M. and Thompson, P. (1980) The Flinton group: a late Precambrian metasedimentary sequence in the Grenville Province of eastern Ontario. *Canadian Journal of Earth Sciences*, **17**, 1685–1707.

Munker, C., Worner, G., Yogodzinski, G. and Churikova, T. (2004) Behaviour of high field strength elements in subduction zones: constraints from Kamchatka-Aleutian arc lavas. *Earth and Planetary Science Letters*, **224**, 275–293.

O'Reilly, S.Y., Griffin, W.L. and Ryan, C.G. (1991) Residence of trace elements in metasomatised spinel lherzolite xenoliths: a proton microprobe study. *Contributions to Mineralogy Petrology*, **109**, 98–113.

Pearce, J.A. (1996) A user's guide to basalt discrimination diagrams. Pp. 79–113 in: *Trace Element Geochemistry of Volcanic Rocks: Appliction for Massive Sulphide Exploration* (D.A. Wyman, editor). Geological Association of Canada, Short Course Notes, **12**.



https://doi.org/10.1180/minmag.2015.079.4.04 Published online by Cambridge University Press

Pearce, J.A. (2008) Geochemical fingerprinting of oceanic basalts with applications to ophiolite classification and the search for Archean oceanic crust. *Lithos*, **100**, 14–48.

Pearce, J.A. and Parkinson, I.J. (1993) Trace element models for mantle melting: application to volcanic arc petrogenesis. Pp. 373–403 in: *Magmatic Processes and Plate Tectonics* (H.M. Prichard, editor). Geological Society of London Special Publication **76**. The Geological Society, London.

Pearce, J.A. and Peate, D.W. (1995) Tectonic implications of the composition of volcanic arc magmas. *Annual Review of Earth and Planetary Sciences*, **23**, 251–285.

Pearce, J.A., Barker, P.F., Edwards, S.J., Parkinson, I.J. and Leat, P.T. (2000) Geochemistry and tectonic significance of peridotites from the south Sandwich arc basin system, South Atlantic. *Contributions to Mineralogy and Petrology*, **139**, 36–53.

Polat, A. and Kerrich, R. (1999) Formation of an Archaean tectonic mélange in the Schreiber–Hemlo greenstone belt, superior Province, Canada: implications for Archaean subduction–accretion process. *Tectonics*, **18**, 733–755.

Polat, A. and Kerrich, R. (2002) Nd-isotope systematics of ~2.7 Ga adakites, magnesian andesites, and arc basalts, Superior Province: evidence for shallow crustal recycling at Archean subduction zones. *Earth and Planetary Science Letters*, **202**, 345–360.

Polat, A. and Munker, C. (2004) Hf-Nd isotope evidence for contemporaneous subduction processes in the source of late Archaean arc lavas from the Superior Province, Canada. *Chemical Geology*, **213**, 403–429.

Powell, R. (1984) Inversion of the assimilation and fractional crystallization (AFC) equations; characterization of contaminants from isotope and trace element relationships in volcanic suites. *Journal of the Geological Society*, **141**, 447–452.

Ray, J., Saha, A., Koeberl, C., Thoni, M., Ganguly, S. and Hazra, S. (2013) Geochemistry and petrogenesis of Proterozoic mafic rocks from East Khasi Hills, Shillong Plateau, Northeastern India. *Precambrian Research*, **230**, 119–137.

Rivers, T., 1997. Lithotectonic elements of the Grenville province: review and tectonic implications. *Precambrian Research*, **86**, 117–154.

Rock, N.M.S. (1991) *Lamprophyres*. Blackie and Son, Glasgow, UK, 285 pp.

Roeder, P.L. and Emslie, R.F. (1970) Olivine-liquid equilibrium. *Contributions to Mineralogy and Petrology*, **29**, 275–289.

Rollinson, H.R. (1993) *Using Geochemical Data: Evaluation, Presentation, Interpretation*. Addison Wesley Longman, Harlow, UK.

Shellnutt, J.G. and MacRae, N.D. (2012) Petrogenesis of the Mesoproterozoic (1.23 Ga) Sudbury dyke swarm and its questionable relationship to plate separation. *International Journal of Earth Sciences*, **101**, 3–23.

Söderlund, U., Elming, S,-Å., Ernst, R.E. and Schissel, D. (2006) The Central Scandinavian Dolerite group – protracted hotspot activity or back-arc magmatism? Constraints from U-Pb baddeleyite geochronology and Hf isotopic data. *Precambrian research*, **150**, 136–152.

Sun, S.-S. and McDonough, W.F. (1989) Chemical and isotopic systematics of oceanic basalts: implications for mantle composition and processes. Pp. 313–345 in: *Magmatism in the Ocean Basins* (A.D. Saunders and M.J. Norry, editors). Geological Society of London Special Publication **42**. Geological Society, London.

Taubald, H., Morteani, G. and Satir, M. (2004) Geochemical and isotopic (Sr, C, O) data from the alkaline complex of Grønnedal-Ika (South Greenland): evidence for unmixing and crustal contamination. *International Journal of Earth Sciences*, **93**, 348–360.

Turner, S., Hawkesworth, C.J., Gallagher, K., Stewart, K., Peate, D.W. and Mantovani, M. (1996) Mantle plumes, flood basalts, and thermal models for melt generation beneath continents: Assessment of a conductive heating model and application to the Paraná. *Journal of Geophysical Research*, **101(B5)**, 11503–11518.

Upton, B.G.J. (1991) Gardar-age mantle xenoliths: Igdlutalik, S. Greenland. *Rapport Grønlands Geologiske Undersøgelse*, **150**, 37–43.

Upton, B.G.J. (2013) *Tectono-magmatic evolution of the younger Gardar southern rift, South Greenland.* Geological Survey of Denmark and Greenland Bulletin **29**. GEUS, Copenhagen.

Upton, B.G.J. and Emeleus, C.H. (1987) Mid-Proterozoic alkaline magmatism in southern Greenland. Pp. 449–471 in: *Alkaline Igneous Rocks* (J.G. Fitton and B.G.J. Upton, editors). Blackwell Scientific Publications, Oxford, UK.

Upton, B.G.J., Emeleus, C.H., Heaman, L.M., Goodenough, K.M. and Finch, A. (2003) Magmatism of the mid-Proterozoic Gardar Province, South Greenland: chronology, petrogenesis and geological setting. *Lithos*, **68**, 43–65.

Upton, B.G.J., Craven, J.A. and Kirstein, L.A. (2006) Crystallisation of mela-aillikites of the Narsaq region, Gardar alkaline province, South Greenland and relationships to other aillikitic-carbonatitic associations in the province. *Lithos*, **92**, 300–319.

Walton, B.J. (1963) *Field map with indicated geological observations*. GEUS map archive: 61 V.3 34b. GEUS, Copenhagen.

Wegmann, C.E. (1938) *Geological investigations in southern Greenland. Part 1. On the structural*



https://doi.org/10.1180/minmag.2015.079.4.04 Published online by Cambridge University Press

*divisions of southern Greenland*. Meddelelser om Grønland, **113**. GEUS, Copenhagen, 148 pp.

White, R.S. and McKenzie, D. (1989) Magmatism at rift zones: the generation of volcanic continental margins and flood basalts. *Journal of Geophysical Research*, **97**, 7685–7729.

Winchester, J.A. and Floyd, P.A. (1977) Geochemical classification of different magma series and their differentiation products using immobile elements. *Chemical Geology*, **20**, 325–343.

Wood, D.A. (1980) The application of a Th-Hf-Ta diagram to problems of tectonomagmatic classification and to establishing the nature of crustal contamination of basaltic lavas of the British Tertiary volcanic province. *Earth and Planetary Science Letters*, **50**, 11–30.

Woodhead J., Eggins S. and Gamble J. (1993) High field strength and transition element systematics in island arc and back arc basin basalts: evidence for multi-phase melt extraction and a depleted mantle wedge. *Earth and Planetary Science Letters*, **114**, 491–504.

Woodhead, J.D., Hergt, J.M., Davidson, J.P. and Eggins, S.M. (2001) Hafnium isotope evidence for 'conservative' element mobility during subduction zone processes. *Earth and Planetary Science Letters*, **192**, 331–346.

Wyman, D. and Kerrich, R. (2009) Plume and arc magmatism in the Abitibi Subprovince: implications for the origin of Archean continental lithospheric mantle. *Precambrian Research*, 168, 4–22.

Wyman, D.A., Bleeker, W. and Kerrich, R. (1999) A 2.7 Ga komatiite, low-Ti tholeiite, arc transition, and inferred protoarc geodynamic setting of the kidd creek deposit: evidence for adakitic metasomatism above an Archean subduction zone. *Earth and Planetary Science Letters*, **179**, 21–30.



https://doi.org/10.1180/minmag.2015.079.4.04 Published online by Cambridge University Press